



POLITECNICO
MILANO 1863

Scuola di Ingegneria Industriale e dell'Informazione

Master School in Mechanical Engineering

**A model to study the effect of mediolateral
vibrations while walking: a preliminary study**

Supervisor: Prof. Marco TARABINI

Co-Supervisor: Eng. Stefano MARELLI

M.Sc. thesis by

Ajith Asokan

ID number: 913523

Academic Year 2020/2021

Acknowledgment

I extend my sincere gratitude to my thesis supervisor **Professor Dr. Marco Tarabini** for granting me the opportunity to work on this thesis under his guidance. His expert advice and vision have been invaluable at every stage of this work. I am grateful to him for introducing me to the field of Bio-mechanics and giving me an interdisciplinary research experience.

I would like to acknowledge the contribution of my thesis co-supervisor **Eng. Stefano Marelli**, whose constant support and direction made this work possible. His expertise in the field of bio mechanics helped me tackle challenging problems during the course of this project. He has been my mentor throughout my master's studies and has inspired me to strive for the best.

I am thankful to the faculty of Industrial and Information Engineering at Politecnico di Milano for providing me with excellent working conditions and much-needed research libraries.

I dedicate this thesis to my beloved parents.

AJITH ASOKAN
Milan, April 2021

Contents

List of Figures	1
List of Tables	5
Abstract.....	7
Introduction: Whole-body vibrations effects	9
Chapter 1: Human models	11
1.1 Lumped parameters model.....	11
1.2 Kinematic Models.....	13
1.3 Direct Kinematics Computation Method	13
1.4 Inverse Kinematics Computation Method.....	15
1.5 Dynamic Models.....	15
1.6 Model simulating walking muscular activation	15
Chapter 2: Simulation environments for human models	17
2.1 ADAMS	17
2.2 AnyBody	18
2.3 SimWise – 4D.....	18
2.4 Simbody.....	19
2.5 Open Dynamics Engine (ODE).....	20
Chapter 3: Musculoskeletal model implementation	21
3.1 Newton Dynamics Engine	21
3.2 Newton dynamics engine description.....	22
3.3 Flow chart of model newton engine	22
3.3.1 DGVehicleRCManager	23
3.3.2 NewtonManager.....	24
3.3.3 WindowGL	24
3.4 Anthropometric data.....	25
3.4.1 Lengths of body segments.....	25
3.4.2 Inertia of body segments.....	29
3.5 Mechanical model definition in Newton Dynamics Engine	30
3.6 Lower limbs activation	36
3.6.1 Muscle force based on Newton-Raphson algorithm.....	36
3.6.2 Muscle force computation by solving the inner degree of freedom of Hill-type Musculotendon Unit	38
3.6.3 Properties of muscle in literature.....	42

3.7	Muscle definition in Newton Dynamics Engine	44
Chapter 4: data analysis and actuation simulation		45
4.1	Anthropometric data comparison.....	45
4.2	Muscle data comparison	48
4.3	Experiments on lower limbs activation.....	50
4.4	Monoarticular muscle output parameters from the simulations	52
4.4.1	Output of the five monoarticular muscle groups using length integration method	52
4.4.2	Output of HFL using velocity integration method.....	58
4.5	Effect of change in position of the origin point.....	59
4.6	Effect of delay between nervous excitation and muscular activation	63
Chapter 5: Conclusions and future developments		65
5.1	Conclusions	65
5.2	Future developments	66
Bibliography		67
Appendix		70
Input XML file containing the muscle and body segment data		70

List of Figures

Figure 1 Schematic of one degree of freedom without support (a), one degree of freedom with massless support (b) and two degrees of freedom models (c, d, e, f) used by Matsumoto and Griffin [6]. Source: <i>Journal of Sound and Vibration</i> 260 (2003) 431–451.....	11
Figure 2 Multiple degrees of freedom models representing knees stretched (a) and bent positions (b) used by Subashi et al. Source: <i>Journal of Sound and Vibration</i> 317 (2008) 400–418	12
Figure 3 Chadeaux et al's lumped parameter model of a foot consisting of rearfoot (I), midfoot (II), forefoot (III) and toes (IV) segments. Source: <i>Journal of Biomechanics</i> 99 (2020) 109547	13
Figure 4 Musculoskeletal model of Wang et al (left), Schematic of uniarticular muscles (middle) and schematic of biarticular muscles (right). Source: <i>ACM Trans Graph.</i> 2012 July 31(4): doi:10.1145/2185520.2185521.....	16
Figure 5 Full body multibody model of the patient with the prosthetic knee during a forward dynamics gait simulation. The red arrows represent the magnitude of joint contact forces and ground reaction forces. Source: <i>Med Eng Phys.</i> 2014 March ; 36(3): 335–344. doi:10.1016/j.medengphy.2013.12.007.	17
Figure 6 Musculoskeletal model getting out of a car. Source: AnyBody Modeling System. https://www.anybodytech.com/software/ams/	18
Figure 7 (a) Swing kinematics when reducing the RF force; (b) swing kinematics resulting from increasing the RF force. These 10 simulations were obtained at an interval of 100 percent of stride time. The red trajectory describes the motion of the left heel while the blue indicates the trajectory of the right heel. Source: <i>Appl. Sci.</i> 2020, 10(21), 7881; https://doi.org/10.3390/app10217881	19
Figure 8 Protein model that is simulated inside Simbody engine. Source: Simbody 2.2 Documentation. https://simtk.org/docman/?group_id=47	19
Figure 9 Humanoid model musculoskeletal gait simulation inside Open Dynamics Engine by Wang et al. Source: <i>ACM Trans Graph.</i> 2012 July ; 31(4): . doi:10.1145/2185520.2185521..	20
Figure 10 Hexapod walker (demo) run inside Newton Dynamics engine. Source: Newton Dynamics (demosandsandbox project).....	21
Figure 11 Process flow of the program inside Newton Dynamics engine	23
Figure 12 The Newton Dynamics window running the gait simulation.	25
Figure 13 Body segment lengths expressed as a factor of total height (H). Source: <i>Biomechanics and Motor Control of Human Movement: Fourth Edition.</i> https://doi.org/10.1002/9780470549148	26
Figure 14 Sketch of the front (Vertical: Z and Horizontal: Y axes) and the side (Vertical: Z and Horizontal: X axes) profile of Wang's model. The origin is taken as the trunk (red point).....	26
Figure 15 Parent child hierarchy of the segments. The sacrum is the root parent. The orange dots represent double hinge joint, the green ones represent ball and socket joints, and the	

blue ones indicate hinge joints. There are 15 unique joints which makes a total of 27 joints when counting both the left and right sides. 33

Figure 16 The three joint class types used to connect the body segments: A) dCustomHinge allows motion only along one axis; B) dCustomDoubleHinge allows rotation in 2 axes; C) dCustomBallAndSocket joint allows rotation along all the three axes..... 33

Figure 17 Hill-type muscle model showing the lengths l_{CE} , l_{SE} and l_m , and of the contractile element, serial element and entire musculotendon unit respectively. $f^n(t)$ is the force exerted by the entire muscle unit at a time t 36

Figure 18 Type Hill's muscle with contractile element (CE), higher parallel elasticity (HPE), lower parallel elasticity (LPE) and series elasticity (SE). 39

Figure 19 Nine muscle group model developed by Reiner and Fuhr. The spring damper system represents forces involved in body seat interaction. The two forces and one moment at the shoulder represent the control actions of the neurologically intact upper body. The values of φ_H , φ_K and φ_A represent the angles at the hip, knee and ankle respectively. Source: IEEE Transactions on Rehabilitation Engineering, 6(2), 113–124. <https://doi.org/10.1109/86.681177> 43

Figure 20 Comparison between body segment lengths given by Winter, Wang and Leva..... 45

Figure 21 Comparison of Wang and Leva models' logarithmic values of inertia in transverse, longitudinal and sagitta planes for the eight body segments. The maximum difference is observed in the inertia of trunk, for all the three directions..... 46

Figure 22 Comparison of mass percentages of segments given by Leva, Wang and Brunner 47

Figure 23 Body segments (red points) and their connecting joints (yellow points) whose data are in table 1 47

Figure 24 Initial model built in Newton Dynamics engine using the Human model data used by Leva. Lengths (left) and mass distribution (right) for the segments. The model has a total mass of 73 kg and each segment has its mass expressed as % of total mass and is located at its centre of mass (COM)..... 48

Figure 25 Comparison of Geyer's and Reiner's data for maximum muscle force exerted. The differences in muscle force has been highlighted above each muscle group's bar 49

Figure 26 Comparison of Geyer's and Reiner's data for maximum velocities. The differences in maximum muscle velocity has been highlighted above each muscle group's bar 49

Figure 27 Comparison of Geyer's and Reiner's data for optimum muscle lengths. The differences in optimum muscle lengths has been highlighted above each muscle group's bar 50

Figure 28 Cyclic contraction and expansion of the muscle fiber attached to two segments due to external activation..... 50

Figure 29 Normalized muscle component forces f_{SE} , f_{CE} and f_{PE} along with the variation in the length of contractile element plotted against time. 51

Figure 30 f_{SE} , f_{CE} , f_{PE} and l_{CE} plotted for one cycle of contraction and expansion. The minimum value of f_{CE} , coincides with that of f_{SE} 51

Figure 31 Initial and final position of the leg after activating the SOL muscle..... 53

Figure 32 Force exerted by the SOL muscle group's contractile element plotted with length of CE due to activation of value 1	53
Figure 33 Initial and final position of the leg after activating the TA muscle	54
Figure 34 Force exerted by the TA muscle group's contractile element plotted with length of CE due to an activation of value 1	54
Figure 35 Initial and final position of the leg after activating the VAS muscle. The black dotted line used to denote the distance of the origin point from the centre of mass of the segment.....	55
Figure 36 Force exerted by the VAS muscle group's contractile element plotted with length of CE due to activation of value 1	55
Figure 37 Initial and final position of the leg after activating the GLU muscle. The black dotted line used to denote the distance of the origin point from the centre of mass of the segment.....	56
Figure 38 Force exerted by the GLU muscle group's contractile element plotted with length of CE due to activation of value 1	56
Figure 39 Initial and final position of the leg after activating the HFL muscle. The black dotted line used to denote the distance of the origin point from the centre of mass of the segment.....	57
Figure 40 Force exerted by the HFL muscle group's contractile element plotted with length of CE due to activation of value 1	57
Figure 41 Force exerted by HFL musculotendon unit and the length of its contractile element plotted against time, computed using velocity integration method	58
Figure 42 Positions of the origin point of VAS chosen for the four trials. The original origin point has been denoted with position '0', which is below (X-direction) the centre of mass of the thigh by 0.15 m and behind (Z-direction) by 0.07 m. Note: the coordinate system mentioned in this figure is tilted when compared to the global coordiante system as the upper and lower leg segments are rotated by 90° during their creation. COM _T and COM _S denote the centre of mass position of the thigh and the shank respectively.	59
Figure 43 VAS muscle's contractile element (CE) force and length comparison when the origin point is behind by 5 cm (in the Z direction). The values of forces and lengths for of the CE for the original trial '0' have been plotted as dotted lines.	60
Figure 44 VAS muscle's contractile element (CE) force and length when the origin point is closer to the thigh (by 5 cm in Z direction) compared to the original position. The values of forces and lengths for of the CE for the original trial '0' have been plotted as dotted lines. ...	60
Figure 45 VAS muscle's contractile element (CE) force and length when the origin point is moved up by 5 cm in the X direction. The values of forces and lengths for of the CE for the original trial '0' have been plotted as dotted lines.	61
Figure 46 VAS muscle's contractile element (CE) force and length when the origin point is below the original position by 5 cm (in the X direction). The values of forces and lengths for of the CE for the original trial '0' have been plotted as dotted lines.	61
Figure 49 Nervous excitation and muscular activation for a step size of 1/10000 s.....	63

Figure 50 Force exerted by VAS contractile element plotted, for a step size of $1/10000$ s. The dotted line indicates the curve of f_{CE} when there is no delay.64

Figure 51 Length of VAS' contractile element plotted for a step size of $1/10000$ s. The dotted line indicates the curve of l_{CE} when there is no delay.64

List of Tables

Table 1 Anatomical segment definition with the primary axis (green, labelled line), rotation reference point (green, labelled point) and marker placement (yellow points) for video capture, for Conventional Gait Model. Source: Handbook of Human Motion. Springer, Cham. https://doi.org/10.1007/978-3-319-14418-4_25	14
Table 2 List of C++ libraries used in the project.	22
Table 3 Comparison of Leva and Winter's segment lengths for a subject height of 1.741 m. 27	
Table 4 Comparison of mass percentages of segments between Leva, Wang and Winter	27
Table 5 Comparison of densities of human model segments of Leva, Wang and Winter. The value of density used in Wang's model has been obtained from Wooten and Hodgins [1996].	28
Table 6 Difference in segment lengths between Frigo et al and Leva's human models. The model used by Frigo et al has a height of 160 cm and has 45 kg of total body mass. Whereas, the model used by Leva has a height of 1.74 m and weighs 61.9 kg.	28
Table 7 Calculation of inertia about the proximal axis for Winter's model.....	29
Table 8 Anthropometric data for masculine subject, of height 1.741 m and 73 kg, used by de Leva. The Centre of Mass is in the X direction: in local coordinate of the body.	30
Table 9 Comparison of Inertia values, of the models' body segments, between Wang and Leva. Inertia values of hip and shoulders are included in the body of the trunk for Leva's model.	30
Table 10 Constraints set on elbows, hip joints and knees. As the hip joint is double hinge, rotation is allowed in the lateral direction.....	34
Table 11 Parent, Child segments with the joints connecting them. $_Pos$ is the initial position of the human model, it is given by the coordinates ($X = 0$, $Y = l_{Sacrum}/2 + l_{Up_Leg} + l_{Low_Leg} + h_{foot} + l_{Hip} + 0.25f$, $Z = 0$), $r_{bones} = 0.07$ m is the radius of the bones.....	35
Table 12 MTU parameters values are estimated from Yamaguchi et al assuming a force of 25 N per cm^2 cross sectional area, maximum velocity of 6 for slow and 12 for medium-fast twitch muscles, and l_{opt} , l_{slack} values to reflect muscle fiber, tendon lengths	42
Table 13 MTU attachment parameters used by Geyer and Herr. Arm length (r_0), φ_{ref} is the reference joint angle at which $l_{mtu} = l_{opt} + l_{slack}$, lever length, $r_m(\varphi) = r_0 \cdot \cos(\varphi - \varphi_{max})$ for the ankle and the knee while $r_m(\varphi) = r_0$ for the hip. ρ accounts for the for muscle pennation angles and ensures that the MTU fiber length stays within the physiological limits throughout the joint work space. Change in the MTU length $\Delta l_{mtu} = \rho r(\varphi - \varphi_{ref})$ for the hip and $\Delta l_{mtu} = \rho r[\sin(\varphi - \varphi_{max}) - \sin(\varphi_{ref} - \varphi_{max})]$ for the angle and knee.....	43
Table 14 Muscle groups and their corresponding maximum isometric force (F_{max}), optimal muscle length (l_{opt}) and maximum contraction velocity (v_{max}) as described by Reiner and Fuhr	44
Table 15 Maximum and minimum values of f_{SE} , f_{CE} , f_{PE} and l_{CE} found from the simulation	52

Table 16 Origin and insertion points along of the eight muscle groups along with the segments which they attach. The coordinates X (horizontal), Y (vertical) and Z (through screen) are measured from the centre of mass of the segments which the muscles attach. .52

Table 17 Maximum value of force of CE and length of CE at the end of the simulation for the trials I-IV in which the origin point's position was moved in different directions.....62

Abstract

A preliminary musculoskeletal model to study the effect of mediolateral vibrations on human body has been implemented in a suitable real-physics simulation environment. Anthropometric data such as the segment lengths, masses and inertias were collected from different studies and compared. The lower limbs have been actuated by 8 type-Hills muscles retrieving data from literature. The Hill-Type model has been tested in two different configurations and approaches. The first method solved the internal degree of freedom of the muscle using internal state variable to perform Newton-Raphson algorithm. The second muscle model instead was solved using numerical integration of the contraction velocity of the muscle. The force given by the HFL muscle obtained from both methods are comparable in terms of maximum force (1600 N) and response time (200 ms for the integration method and 400 ms for the Newton-Raphson method to reach the maximum force). Also, the length contraction was similar for both methods and equal to 5 cm, in accordance with previous developed models.

Introduction: Whole-body vibrations effects

Long term exposure to Whole Body Vibrations (WBV) is known to have a toll on physical and mental wellbeing of a person. The outcomes may vary from lower back pain and dizziness to permanent change in the posture and loss of cognitive abilities. The person subjected to WBV may be stationary (driver operating excavating vehicle in a mining site) or dynamic (operator walking on a shopfloor vibrating due to the machinery). Bovenzi et al conducted a systematic search, using several databases of epidemiological studies on low back pain disorders and occupations with WBV exposure, and reported that up to 7% of all workers in Europe, the United States, and Canada are regularly exposed to WBV. Finally, in the fourth edition of the European Working Conditions Survey (EWCS), it was reported that nearly 24% of all workers in the European Union reported being exposed to vibration at work at least a quarter of the time [1, 2].

The review performed by Nordlund et. al. finds that WBV contributes only in negligible ways when it comes to improving the jump performance and muscle strength in healthy people [3]. These improvements cannot be attributed to WBV with confidence. Studies have been conducted to see if there are positive effects to low amplitude WBV. Lam et al studied the connection between WBV and improved bone growth in adolescent girls with idiopathic scoliosis [4]. They were made to stand on a vibrating platform for 20 minutes a day, 5 days a week for an entire year. When compared with girls of same age (outside the active group) the girls exposed to WBV had showed significant improvement in bone growth.

In literature, different studies have investigated the effects of WBV of standing subjects, and standards have been created to define vibration exposure limits for workers. As for standing subjects, WBV while walking can affect both the walking kinematic and the mechanical response of the subject. To study these effects, experiments with subject walking on an oscillating treadmill have been done [5].

The objective of this thesis is to develop the mechanical and actuation method of a model that simulates the dynamics and kinematics of a walking subject exposed to mediolateral WBV.

In Chapter 1, an overview on models that have been developed to study human response to vibrations and human walking is presented. Then, in Chapter 2, a focus on the simulation environments available is provided. In Chapter 3, the mechanical model of the walking subject is presented and its definition in the physics engine is described. In Chapter 4, the previously described data, from various authors, have been

compared and the results of lower limb actuation have been provided. The conclusions and future developments are presented in the Chapter 5.

Chapter 1: Human models

To study the human response to vibration, different models have been developed. These models can be classified into lumped parameters models, kinematic models, and dynamic models.

1.1 Lumped parameters model

When designing a structure or a mechanical system that interacts with the human body, it is important to understand the dynamic behaviour of the body and the interaction between the structure and the body. Matsumoto and Griffin created six lumped parameter models (two 1 degrees of freedom and four 2 degrees of freedom) to represent a human body in three different postures, undergoing four different magnitudes of vibration [6]. The expressions of apparent masses for these six models are complex functions that consist of the masses, damping and stiffness values. The apparent masses given by these expressions were compared with the apparent masses obtained in an experimental study consisting of 12 test subjects, to obtain the model parameters. The two degrees of freedom models with spring-mass-damper systems either in parallel or series showed good correspondence with the measured data. The schematics of lumped mass systems tested by Matsumoto and Griffin are described in **Figure 1**.

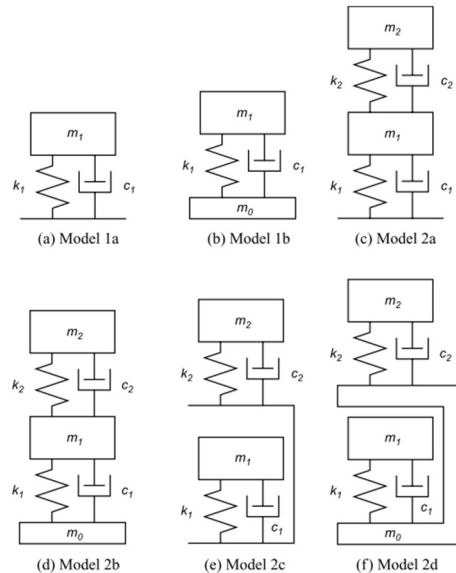


Figure 1 Schematic of one degree of freedom without support (a), one degree of freedom with massless support (b) and two degrees of freedom models (c, d, e, f) used by Matsumoto and Griffin [6]. Source: *Journal of Sound and Vibration* 260 (2003) 431–451

Subashi et al developed lumped parameter models to represent the response of human body, associated with resonances of the vertical and fore and aft cross axis apparent masses, for five different postures [7]. The geometric and inertial data for the models were obtained from previously published anthropometric data. The stiffness and damping parameters were obtained by comparing the mathematical models' responses with the experimental data. Two models having five and seven degrees of freedom respectively were developed. The former model was used to capture the three postures in which knees were unbent while the latter model captured the knees bent and knees more bent scenarios. The second model, when compared to the first, has additional degrees of freedom at the knee (to capture the bent postures) and at the soles of the feet to capture the shear deformation that happens in the fore-aft direction. The multiple degrees of freedom models used by Subashi et al is shown in **Figure 2**.

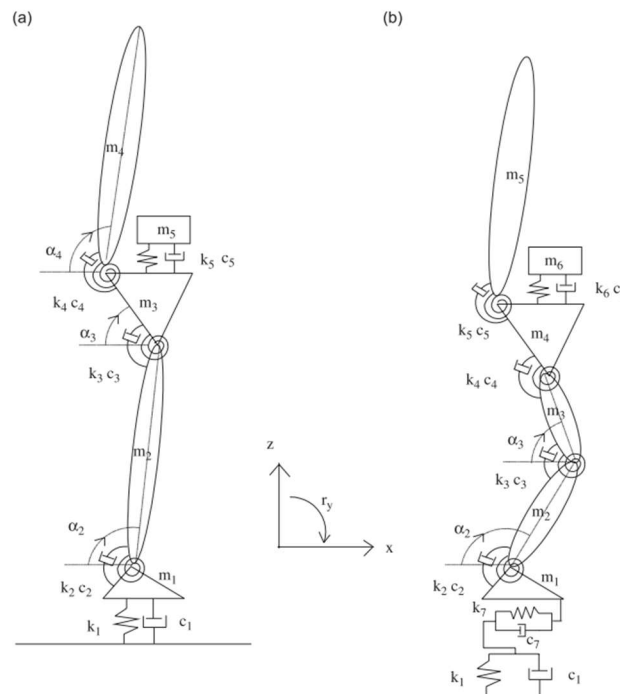


Figure 2 Multiple degrees of freedom models representing knees stretched (a) and bent positions (b) used by Subashi et al. Source: *Journal of Sound and Vibration* 317 (2008) 400–418

Lumped parameter models can also be used to focus on certain parts of the body. Subashi et al proposed a model capable of representing the lower limbs, with an internal oscillator [7]. This allowed the authors to model different postures and study their effect on the modal parameters of the model. Chadeaux et al proposed a lumped parameter model of the foot-ankle system with seven degrees of freedom to study the apparent mass and vibration transmission from the ground to five different parts on a foot [8]. This model consists of four segments and eight Kevin-Voigt models which are shown in **Figure 3**.

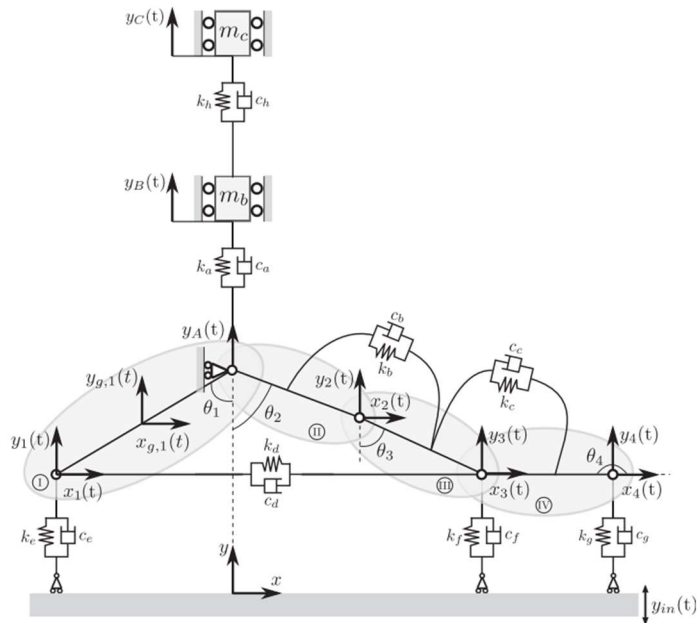


Figure 3 Chadefaux et al's lumped parameter model of a foot consisting of rearfoot (I), midfoot (II), forefoot (III) and toes (IV) segments. Source: *Journal of Biomechanics* 99 (2020) 109547

1.2 Kinematic Models

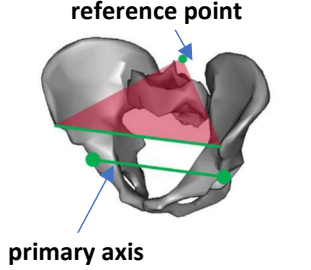
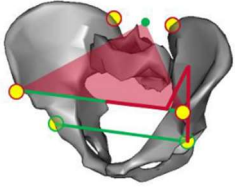
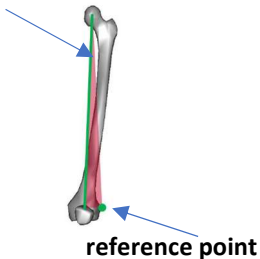
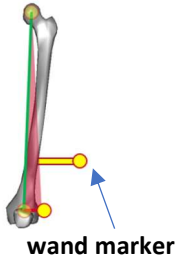
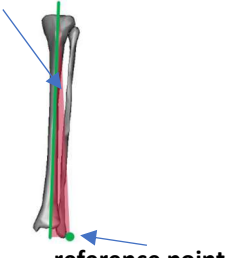
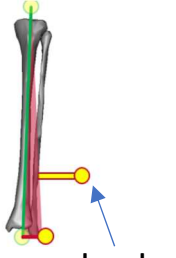
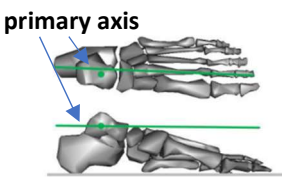
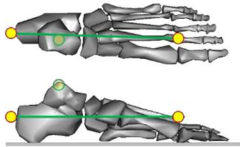
The target of kinematic models is to reconstruct the trajectory of joint angles during walking. In the next sections Direct and Inverse Kinematic methods will be compared.

1.3 Direct Kinematics Computation Method

Conventional Gait Model (CGM) is one of the earliest and commonly used bio mechanical model used in clinical gait studies [9]. Prominent use of this model in clinical studies can be attributed to the ease with which it can be understood, even by non-experts in Biomechanics, and its availability as a package along with Vicon software developed by Vicon (Oxford Industrial Park, United Kingdom).

In Direct Kinematics, the trajectory of motion of a subject wearing photo reflective optical markers is captured using a 3D video capturing technique like Vicon systems. The arrangement of the optical markers varies depending on the Vicon model chosen. Plug-in-Gait (PiG) is a variant of the conventional gait model that is available with the Vicon/Nexus software package [10]. It can capture joint kinematics of the leg, with minimum number of optical markers [11, 12]. At every frame, the cardan angles between the segments of the leg are computed from change in the position of the optical markers with respect to each other. The anatomical segment definitions and marker placement for CGM have been described in **Table 1**.

Table 1 Anatomical segment definition with the primary axis (green, labelled line), rotation reference point (green, labelled point) and marker placement (yellow points) for video capture, for Conventional Gait Model. Source: Handbook of Human Motion. Springer, Cham. https://doi.org/10.1007/978-3-319-14418-4_25

Bone Segment	Anatomical segment definition for the CGM	Marker placement for the CGM	Location of reference points and primary axes
Pelvis	 <p>reference point</p> <p>primary axis</p>		<p>The primary axis is the mediolateral axis that runs from the left hip joint to the right</p> <p>The reference point for rotation about this axis is the mid-point of the posterior superior iliac spines (PSIS).</p>
Femur	 <p>primary axis</p> <p>reference point</p>	 <p>wand marker</p>	<p>The primary axis is that running from the hip joint centre to knee joint centre.</p> <p>The reference point marked is the lateral epicondyle.</p>
Tibia	 <p>primary axis</p> <p>reference point</p>	 <p>wand marker</p>	<p>The primary axis is that running from the knee joint centre to ankle joint centre.</p> <p>The reference point marked is the lateral malleolus.</p>
Foot	 <p>primary axis</p>		<p>The primary axis is that running from the most posterior axis of the calcaneus along the second ray and parallel to the plantar surface of the foot.</p> <p>Rotation about the primary axis is not defined for foot.</p>

1.4 Inverse Kinematics Computation Method

In IK computation method (also known as global optimization), a computer model of a human skeleton is used where position of markers in the model are tried to be matched with the optical markers present in the footage captured and joint kinematics are calculated. This method also allows for errors in the placement of markers.

Wang et al developed a musculoskeletal model which has powered simple Hill-type muscles. 16 muscle groups, eight on each leg worked in coalition to generate torques at the joints in order to generate a stable gait [13]. A virtual marker set was placed on each model based on these same anatomical landmarks. For each trial, inverse kinematics (IK) calculated joint angles and inverse dynamics calculated joint moments (i.e., torques) given joint angles and measured ground reaction forces. Scaling, IK, and inverse dynamics were performed inside a physics-based controller.

1.5 Dynamic Models

Dynamic models' target is to compute muscle load profiles for a given walking pattern. This approach is also used to calculate the metabolic consumption of walking. If the kinetic response model does not yield realistic results, then the predicted muscle loads will be inaccurate, which in turn will calculate energy spent incorrectly [14]. To determine the best gait pattern for a specific velocity, energy spent by the muscles can be used as a parameter. Conversely, the velocity attained is computed when given fixed input energy.

The direct application of torques to the joints, as described in the previous section, ignores constraints and energetic costs imposed by muscle anatomy and physiology [13]. In order to, achieve realistic gait, an optimization criterion of minimum metabolic expenditure was adopted for the muscles. This adoption of minimum energy resulted in biologically realistic torque patterns.

1.6 Model simulating walking muscular activation

In passive models, the effect of muscular activation is not considered because the model parameters are time invariant. Zadpoor et al pointed out that during certain activities like running, passive models fall short as they are unable to reproduce results that are like those of the experiments [15]. Vibration influences muscular activation, so it is useful to simulate muscle and see the effects of vibration on actuation levels.

Wang et al uses a 3D humanoid model of height and weight approximating 180 cm and 70 kg respectively, with 30 joint degrees of freedom [13]. This model uses Hill-Type Musculotendon Units (MTUs) for partial actuation. Gait is predominantly performed by the 8 MTUs for each leg. In addition, soft joint limit torques are applied.

The hip extends with gluteal muscles (GLU) and flexes with hip flexor muscles (HFL), and the vasti (VAS) extends the knee. Dorsiflexion and plantarflexion torque are applied at the ankle by the tibialis anterior (TA) and the soleus (SOL) respectively. These muscles are mono-articular in nature. Whereas the biarticular muscles actuate two different joints at the same time. The hamstring (HAM) extends the hip and flexes the knee, while the rectus femoris (RF), flexes the hip and extends the knee, and the gastrocnemius (GAS), flexes the knee and plantarflexes the ankle. A schematic of the eight muscle group locations alongside the three dimensional model have been described in **Figure 4**.

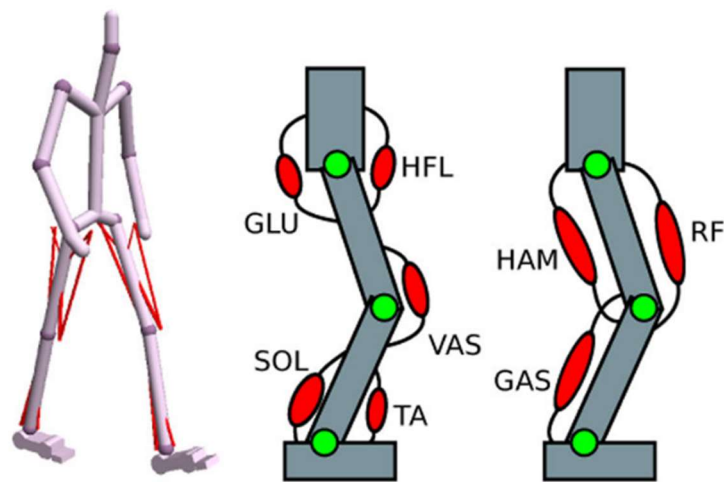


Figure 4 Musculoskeletal model of Wang et al (left), Schematic of uniarticular muscles (middle) and schematic of biarticular muscles (right). Source: ACM Trans Graph. 2012 July 31(4): doi:10.1145/2185520.2185521.

In chapter 2, the various simulation environments, used in literature, for gait simulation have been described.

Chapter 2: Simulation environments for human models

The popularity of physics simulation engines among researchers and developers varies due to various factors like cost, accessibility, ease of use and their computation performance. For biomechanical simulations of complete or a portion of human body, various simulation environments are used. In this section the commonly used physics engines for gait analyses are discussed.

2.1 ADAMS

ADAMS (MSC Software, Irvine, California) is a multibody simulation environment and is used for mechanical simulations. It improves engineering efficiency and reduces product development costs by enabling early system-level design validation. Engineers can evaluate and manage the complex interactions between disciplines including motion, structures, actuation, and controls to better optimize product designs for performance, safety, and comfort. Along with extensive analysis capabilities, Adams is optimized for large-scale problems, taking advantage of high-performance computing environments.

Kia et al uses a full body musculoskeletal model with subject specific lower extremity geometries in ADAMS [16, 17]. This aim of this experiment was to evaluate a musculoskeletal model with knee prosthetics with data from six experimental gait trials. Besides the creation of the model, ADAMS was used for the multibody dynamic analysis. This simulation has been described in **Figure 5**.

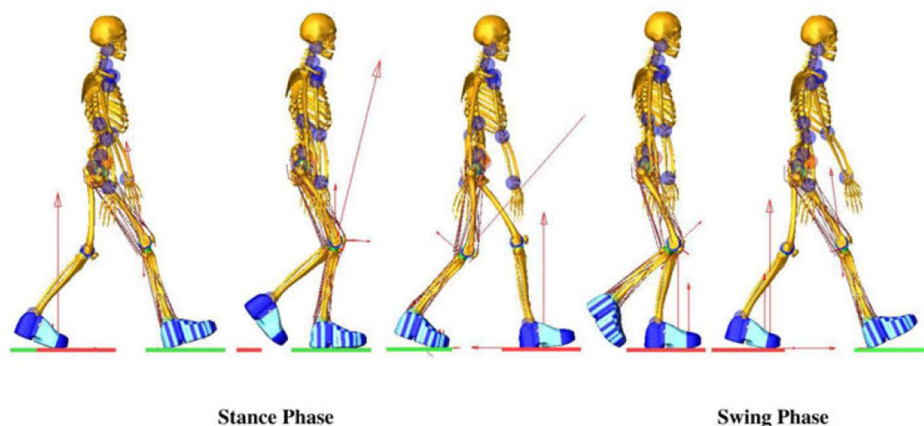


Figure 5 Full body multibody model of the patient with the prosthetic knee during a forward dynamics gait simulation. The red arrows represent the magnitude of joint contact forces and ground reaction forces. Source: *Med Eng Phys.* 2014 March ; 36(3): 335–344. doi:10.1016/j.medengphy.2013.12.007.

2.2 AnyBody

AnyBody (AnyBody Technology A/S, Aalborg, Denmark), used by Brunner et al, offers musculoskeletal models and associated software, simulating the human body working in combination with its external environment [18, 19]. Joint moments and individual muscle forces and muscle power were obtained from the inverse dynamic simulation by importing gait data captured by 12 Vicon motion capture cameras over 6 trials. This study was focused on the rectus femoris (RF) muscle, during walking, to understand the effects of muscle weakness and hyperactivity. The anthropometric data of the model used by Brunner et al is described in the Literature Review section.

AnyBody technology offers a trial version for free while the complete version is priced. An overview of user interface of AnyBody software is shown in **Figure 6**.



Figure 6 Musculoskeletal model getting out of a car. Source: AnyBody Modeling System.
<https://www.anybodytech.com/software/ams/>

2.3 SimWise – 4D

With SimWise 4D, one can simulate the rigid body dynamics of an assembly, size components, determine part interferences and collision response, identify stresses induced by motion, produce physics-based animations, and test control systems. For the forward dynamics simulations of the rectus femoris (RF) muscle, Frigo et al uses SimWise - 4D software (Design Simulation Technologies, Inc., Canton, Michigan) [20]. The force exerted by RF was changed from 0 to 150% and the resulting kinematics were analyzed. The range of motions described due to the changes in force are described in **Figure 7**. This software is available with educational as well as commercial license.

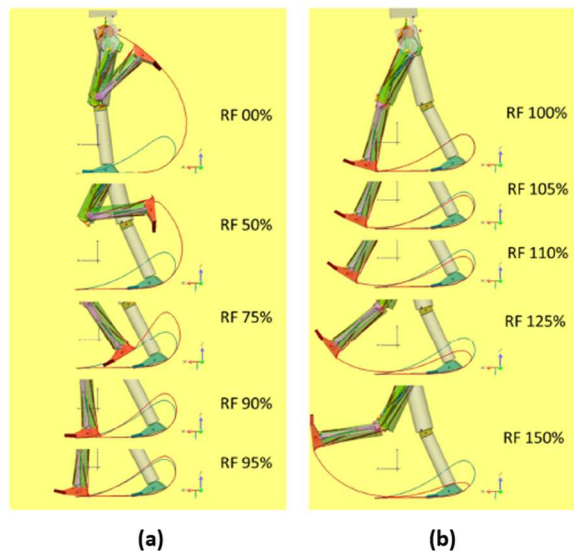


Figure 7 (a) Swing kinematics when reducing the RF force; (b) swing kinematics resulting from increasing the RF force. These 10 simulations were obtained at an interval of 100 percent of stride time. The red trajectory describes the motion of the left heel while the blue indicates the trajectory of the right heel. Source: *Appl. Sci.* 2020, 10(21), 7881; <https://doi.org/10.3390/app10217881>

2.4 Simbody

Simbody (SimTK, Bethesda, Maryland) is a multibody physics API that is useful for modelling internal coordinate, coarse grained molecule, human skeletal model, and any models involving bodies interconnected by joints, with force acting and under constraints [21]. Applications using Simbody have been implemented in areas of biomedical research across a wide range of scales and purposes [22]. This engine provides multibody dynamics ability, in essence, the ability to solve Newton's 2nd law ($F = ma$) in any set of generalized coordinates subject to arbitrary constraints. It is open source, object-oriented C++ and delivers high-performance, accuracy-controlled science/engineering-quality results.

In **Figure 8** is a protein model, mimicking the original protein's behaviour for 10 picoseconds.

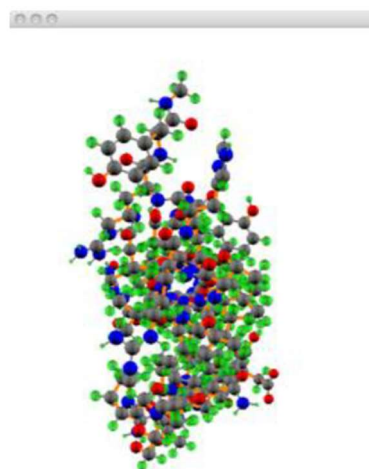


Figure 8 Protein model that is simulated inside Simbody engine. Source: *Simbody 2.2 Documentation*. https://simtk.org/docman/?group_id=47

Simbody is used often in biomechanics through the OpenSim application and in other research areas, where it has proven fast and reliable [23]. OpenSim is a software platform that has a broad set of capabilities ranging from creating and editing models to analyzing and simulating models and motions. An OpenSim model represents the neuromuscular and musculoskeletal dynamics of a human or animal that is of interest to study within a computer simulation. It has various parts like reference frames, bodies, joints, constraints, forces, contact geometry, markers and controllers, which interact together to describe movement.

2.5 Open Dynamics Engine (ODE)

ODE (Russell Smith, Auckland, New Zealand) is a free industry quality engine for simulating articulated rigid body dynamics. It is used, for example, for simulating legged creatures, ground vehicles and moving objects in Virtual Reality environments [24]. Wang et al implemented their simulations using Open Dynamics Engine with a frequency of 2400 Hz. The simulations were performed for 24000 timesteps, which amounts to 10 s, in each evaluation [13]. Wang uses an optimized version of SIMBICON (Simple Biped locomotion CONTroller, developed by Yin et al [25]) to develop a simple control system that can be used to generate a large variety of gaits and styles in real time, that include walking in all directions (forwards, backwards, sideways, turning), running, skipping and hopping. The complete musculoskeletal humanoid model is shown in **Figure 9**.

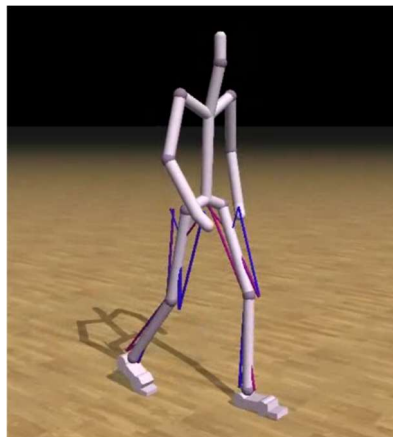


Figure 9 Humanoid model musculoskeletal gait simulation inside Open Dynamics Engine by Wang et al. Source: ACM Trans Graph. 2012 July ; 31(4): . doi:10.1145/2185520.2185521.

In chapter 3, the details regarding the implementation of the muscle groups have been outlined and the anthropometric data along with the muscle parameters, used to create the model, have been described.

Chapter 3: Musculoskeletal model implementation

In this chapter, the virtual environment used to simulate the human model is described. Then, the anthropometric data available in literature have been compared to define the ones used in this thesis. Finally, the model for the activation of lower limbs is described.

3.1 Newton Dynamics Engine

Newton Dynamics is a physics-based game engine that is cross platform, easy to integrate into other applications and light on the hardware usage [26]. Newton Dynamics implements a deterministic solver, which is not based on traditional LCP or iterative methods but possesses the stability and speed of both respectively. This feature makes Newton Dynamics a tool not only for games, but also for any real-time physics simulation.

The fact that Newton Dynamics is open ended and highly customizable also serves as the reason why it is challenging to use and develop simulation environments in. The UI has to be developed from the ground up using an external UI development library. Also, the engine does not offer functions for bio mechanical simulations. Further description on the usage of this engine is described in the next section. An overview of the user interface offered by Newton engine is shown in **Figure 10**.

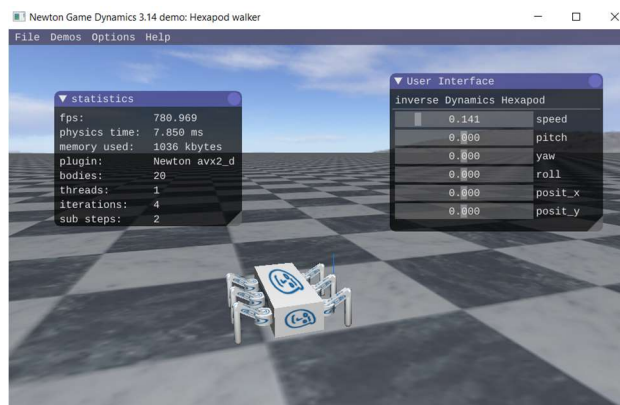


Figure 10 Hexapod walker (demo) run inside Newton Dynamics engine. Source: Newton Dynamics (demosandsandbox project)

Newton Dynamics is the engine that is used in this project due to the following reasons:

- Light and robust performance due to its implementation in C++.
- Open source and commonly used for physics simulations by game developers and researchers.
- The memory usage of Newton Dynamics is optimized.

3.2 Newton dynamics engine description

Newton Dynamics is a cross-platform life-like physics simulation C++ library [26]. It offers basic shapes like sphere, cuboids and capsules which can be linked with each other by means of a joint. Assets can be imported from a wide range of formats using an asset importer package. The degrees of freedom of these joints are customizable and the joint or the hinge can even be set as a motor to achieve rotational motion of a fixed angular speed. Surfaces can be created for these objects which respond to friction and viscosity. These objects can also be given mass, centre of mass and moments of inertia in the three axes. The various software libraries used in this study are described in **Table 2**.

Table 2 List of C++ libraries used in the project.

Library	Details	Download URL
Newton Dynamics	Physics engine [26]	https://github.com/MADEAPPS/newton-dynamics/
Tinyxml	XML reader and writer [27]	https://sourceforge.net/projects/tinyxml/
ImGui	GUI making tool for game engines [28]	https://github.com/ocornut/imgui
OpenGL Extension Wrangler Library (GLEW)	Queries and loads OpenGL extensions [29]	http://glew.sourceforge.net/
Graphics Library Framework (GLFW)	Creates and manages windows and OpenGL contexts, as well as handles joystick, keyboard and mouse input. [30]	https://www.glfw.org/download
OpenGL Mathematics (GLM)	Mathematics library for graphics programming [31]	https://github.com/g-truc/glm

The model developed by Wang et al, was able to attain an efficient walking gait after 10000 cycles of training. With the help of Newton Dynamics, a more efficient model that requires less training time can be developed.

3.3 Flow chart of model newton engine

The properties of the model like segment lengths, masses, moments of inertia and COM can be imported from an external xml file and can be set inside the program. Each segment is a dynamic body which is connect to the adjacent segment by means of a double hinge, ball and socket or normal hinge joints. Lines are projected from the feet to the ground for to serve as a visual and to interpret the distance of the feet from the ground. The eight hill type muscles are created for the left and the right legs with respect to their origin and insertion points which are detailed in the 'Properties of muscle in literature' section.

At every frame, 16 muscles are iterated through, force applied by the muscle is calculated depending on the activation applied at that moment and this elastic force

is applied to the segments the muscle is connected to. At every frame, the value of L_{CE} is calculated and updated.

The program runs continuously in the loop until it is exited. A simplified process flow of Newton Dynamics engine is described in **Figure 11**.

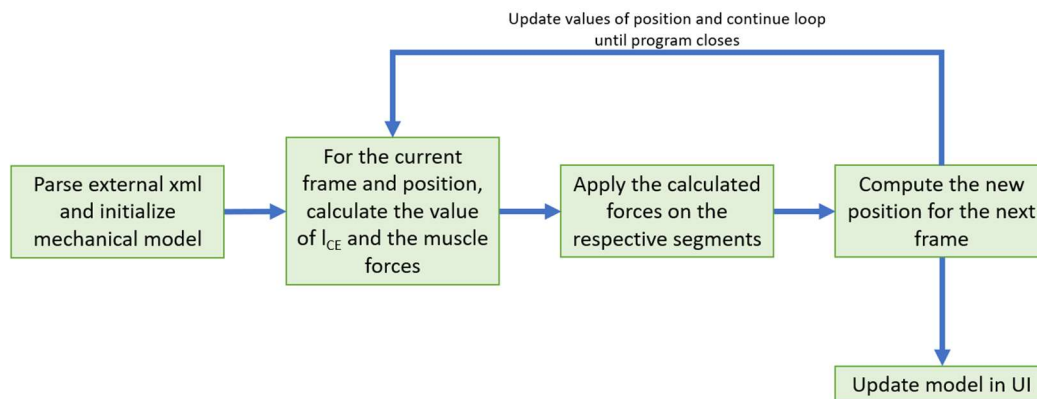


Figure 11 Process flow of the program inside Newton Dynamics engine

In the next sections, three classes used in the simulation environment are described.

3.3.1 DGVehicleRCManager

As the name suggests, DGVehicleRCManager is the manager class which handles dRaycastVHModel. It contains methods which are responsible for updating the model at every frame and calling the functions that are involved in the calculation and application of forces by the muscles. It contains the following methods:

- 'OnPreUpdate': Iterates through every muscle, calculates the forces and applies them on the segments. In the end, the new ICE is calculated by adding the previous ICE with the newly computed ΔICE .
- 'OnPostUpdate': After the model is updated in the frame, rays are projected from the feet to the ground in order to monitor the distance of the model from the floor continuously.
- 'OnUpdateTransform': The method that updates the position and rotation at every frame.
- OnDebug: Contains functionalities that can be used during the debug mode (that is applicable only for the developers).

3.3.2 NewtonManager

Similar to DGVehicleRCManager, NewtonManager class contains helper functions which help with the running the simulation. It contains the following methods:

- CalculateFPS: Calculates the current rate at which the frame is being updated.
- GetFps: A method to retrieve the calculated FPS.
- GetPhysicTime: Returns the main thread physics time.
- PhysicsApplyGravityForce: Retrieves the mass and inertia values of a body and clamps high angular velocities
- SetExcitationList: Sets the values of excitations for the 16 muscle groups.
- UpdateNewton: Update the physics of the simulation for every timestep.
- Render: Renders the asset meshes, geometry and muscles in the simulation

3.3.3 WindowGL

The WindowGL class contains methods to obtain data and manipulate the User Interface of the gait simulation in Newton Dynamics Engine (NDE). Its methods have been described below:

- MainLoop: Inside this method, we create, initialize and update the UI of the NDE. The window to test the muscle excitations of the 16 muscle groups have been written here. This method has a loop, which will keep the window open and update the UI of every frame, and exits the loop only on closing the simulation.
- InitGLRender: This method initializes the OpenGL parameters, creates and sets up the position of Camera.
- MainRender: Updates mouse input to change the camera position and renders the scene.
- ContextResize: Resizes the Window
- ContextKeyPress: Closes the engine window on pressing Escape button.
- ContextMouseButton: Captures mouse button input.
- ContextMouseMove: Captures the movement of the mouse and translates it to camera
- ContextMouseScrl: Captures the scroll input of the mouse.
- SetUseMouseViewRotation: Method that allows camera rotation with mouse.
- GetMouseButton: Returns true if left-click is pressed.
- GetMouseButtonaction: Returns true if any mouse input has been give.
- GetMouseButtonmods: Returns true if the mouse button has been modified.
- GetMouseMoveX: Returns the value of the horizontal change in position of the mouse.
- GetMouseMoveY: Returns the value of the vertical change in position of the mouse.
- GetMousePicking: Returns the variable containing all the actions performed on the mouse.

- GetCamera: Returns the camera object which is to be updated at every relevant mouse input.

In **Figure 12**, the overall user interface of the engine running simulation has been described.

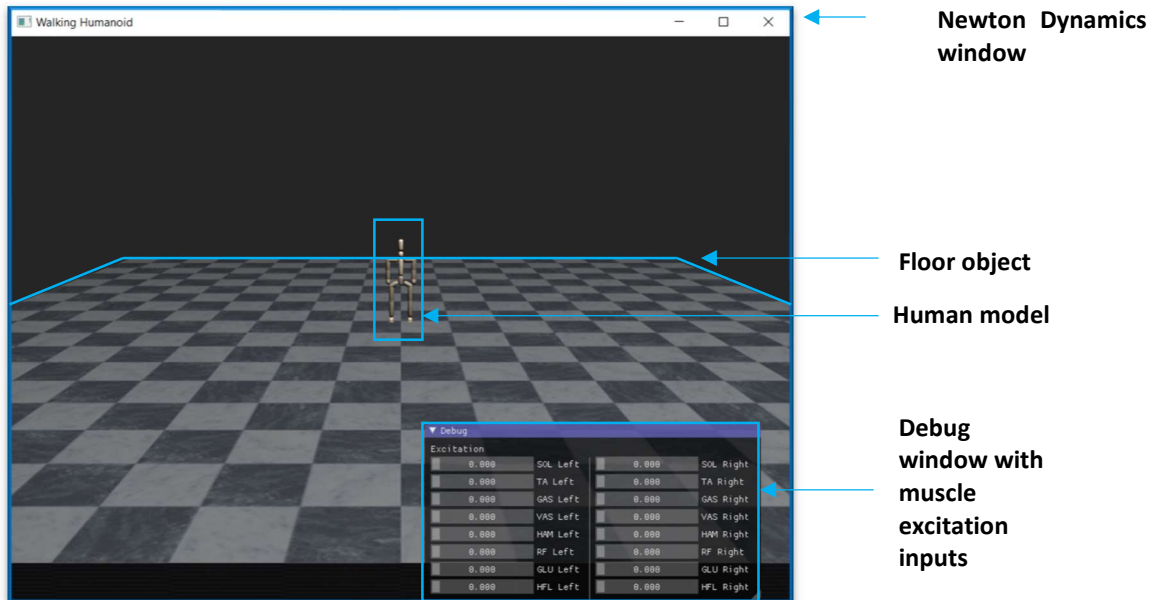


Figure 12 The Newton Dynamics window running the gait simulation.

3.4 Anthropometric data

In this section, the anthropometric properties of body segments like lengths, center of mass and inertia values were retrieved from literature. Data from different sources have been compared.

3.4.1 Lengths of body segments

To properly dimension the musculoskeletal model, anthropometric data were found in literature. Many studies collected data such as mass, length and inertia from Caucasian cadavers in the 20th century [32, 33]. A detailed review of available anthropometric data was done by Leva and Dumas [34, 35] to adjust measurement collected by earlier works by Zatsiorsky, McConville and Young.

Hanavan proposed a model of human body composed of different rigid bodies, in earlier times Wooten and Hodings proposed a model for human diving, giving more detail on human segments [36, 37]. Recently, Geyer proposed a legged model, to model bouncing gaits like hopping and running [38]. In this field, different human walking models have been developed in different simulation environments. Wang proposed a walking musculoskeletal model developed in a three-dimensional simulation environment, composed of rigid elements and muscles [13].

Since, the lengths of segments vary from person-to-person, Winter suggests segment lengths expressed as the percentage body height (as shown in **Figure 13**). This length expression is a good approximation when there is not adequate segment data [40].

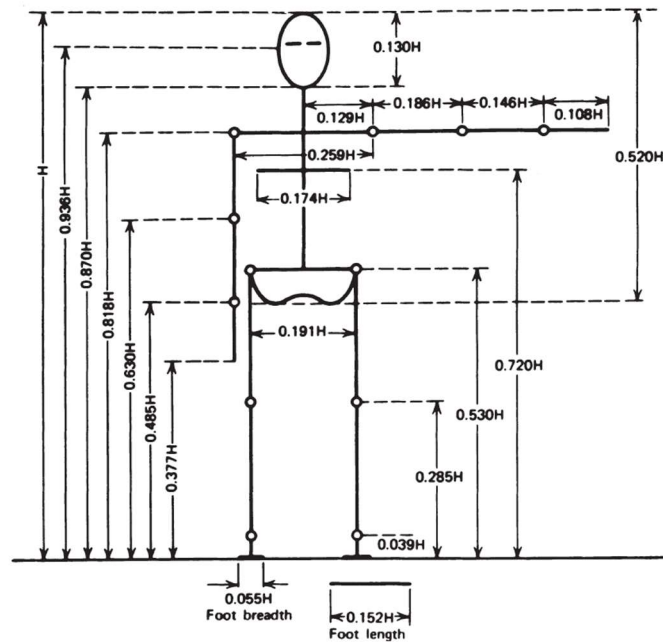


Figure 13 Body segment lengths expressed as a factor of total height (H). Source: *Biomechanics and Motor Control of Human Movement: Fourth Edition*. <https://doi.org/10.1002/9780470549148>

The profile of Wang's body segment lengths have been plotted in **Figure 14**.

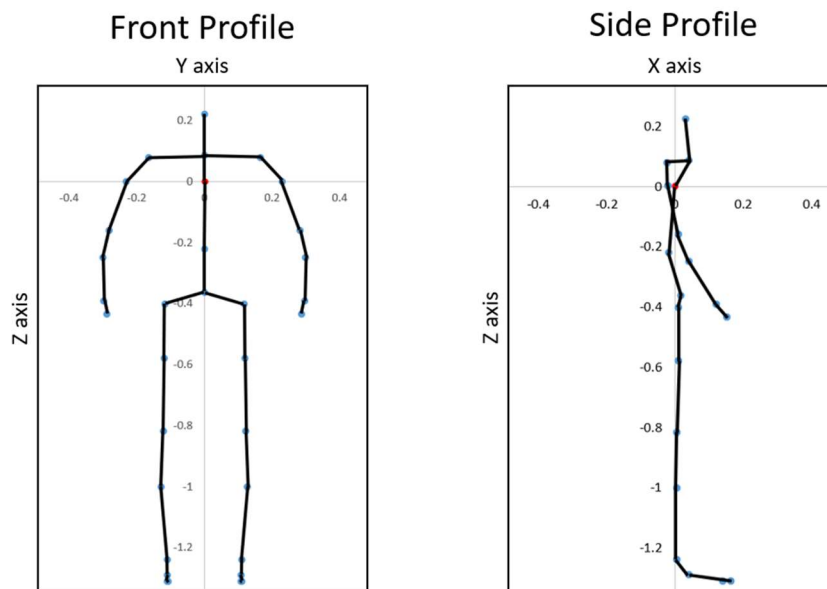


Figure 14 Sketch of the front (Vertical: Z and Horizontal: Y axes) and the side (Vertical: Z and Horizontal: X axes) profile of Wang's model. The origin is taken as the trunk (red point).

To compare the segment lengths of Winter and Leva, in **Table 3** below, the height of the subject is taken as 1.741 meters as defined by Leva. The lengths of Wang's model segments shown in **Figure 4** have been presented in the aforementioned table.

Table 3 Comparison of Leva and Winter's segment lengths for a subject height of 1.741 m.

Segment	Length factor (LF)	Winter segment lengths (L_{Winter}) = LF*H [m]	Wang segment lengths (L_{Wang}) [m]	De Leva segment lengths (L_{Leva}) [m]	Range ($L_{min} - L_{max}$) [m]
Head	0.13	0.23	0.14	0.20	0.14 – 0.23
Arm	0.19	0.32	0.27	0.28	0.27 – 0.32
Forearm	0.15	0.25	0.26	0.27	0.25 – 0.27
Hand	0.11	0.19	0.05	0.09	0.05 – 0.19
Trunk	0.29	0.50	0.59	0.53	0.50 – 0.59
Thigh	0.25	0.43	0.42	0.42	0.42 – 0.43
Shank	0.25	0.43	0.42	0.43	0.42 – 0.43
Foot	0.15	0.26	0.17	0.26	0.17 – 0.26
Hip	0.19	0.33	0.24	0.30	0.23 – 0.33
Shoulders	0.26	0.45	0.33	0.45	0.33 – 0.45

The maximum difference of 0.14 m in length is observed when comparing the hand models, which may be because of the difference in finger lengths.

Mass percentages of segments given by Leva, Wang, Winter and Brunner have been shown in **Table 4**.

Table 4 Comparison of mass percentages of segments between Leva, Wang and Winter

Segments	Percentage of the total body mass				Range ($M_{min} - M_{max}$) [%]
	M_{Leva} [%]	M_{Wang} [%]	M_{Winter} [%]	$M_{Brunner}$ [%]	
Head	6.94	6.2	8.1	7.3	6.2 - 8.1
Arm	2.71	2.96	2.8	2.6	2.6 – 2.96
Forearm	1.62	1.59	1.6	2.3	1.59 – 2.3
Hand	0.61	0.49	0.6	-	0.49 – 0.61
Trunk	43.46	28.19	49.7	34.4	28.19 – 49.7
Thigh	14.16	11.54	10	10.3	10 – 14.6
Shank	4.33	4.6	4.65	4.4	4.33 – 4.65
Foot	1.37	1.67	1.45	1.5	1.37 – 1.67

The mass of head is more for Winter's model as the value includes the mass of the neck. The model of Wang has the least weighing trunk as it does not include the shoulders and hips. The masses of forearm and hand have been combined for $M_{Brunner}$, hence the higher mass percentage.

The densities of the body segments given by Wang and Winter have been compared in **Table 5**.

Table 5 Comparison of densities of human model segments of Leva, Wang and Winter. The value of density used in Wang’s model has been obtained from Wooten and Hodgins [1996].

Segments	d_{Wang} [g/cc]	d_{Winter} [g/cc]	$\Delta d = d_{Wang} - d_{Winter}$ [g/cc]
Head	1.17	1.11	0.06
Arm	1.07	1.07	0.00
Forearm	1.10	1.13	-0.03
Hand	1.07	1.16	-0.09
Trunk	1.01	1.03	-0.02
Thigh	1.04	1.05	-0.01
Shank	1.08	1.09	-0.01
Foot	1.07	1.1	-0.03

The density values between Wang and Winter’s model have the maximum difference (a magnitude of 0.09 g/cc) for hand.

Brunner et al use a human model, with mass and size parameters (Table 9), to study the effects of plantarflexion on pelvis and lower limb kinematics [19]. The same thirteen segments were used by Frigo et al to study the effects of the Rectus Femoris (RF) muscle on the knee and foot kinematics during the swing phase of normal walking, with some adjustments [39]. Differences between Brunner’s and de Leva’s segment lengths have been shown in **Table 6**.

Table 6 Difference in segment lengths between Frigo et al and Leva’s human models. The model used by Frigo et al has a height of 160 cm and has 45 kg of total body mass. Whereas, the model used by Leva has a height of 1.74 m and weighs 61.9 kg.

Body Segment	Size Parameters				L_{Leva} [m]	$\Delta L_{Segment}$ [m]
	Length (l) [m]	Width (w) [m]	Radius (r) [m]	Height (h) [m]		
Head	-	-	0.10	-	0.20	$L_{Leva} - 2 \times r = 0.00$
Trunk	0.18	0.30	-	0.30	0.53	$L_{Leva} - h = 0.23$
Pelvis	0.12	0.24	-	0.16		-
Upper arm			0.04	0.28	0.28	$L_{Leva} - h = 0.00$
Forearm			0.035	0.30	0.27	$L_{Leva} - h = -0.03$
Thigh			0.06	0.35	0.42	$L_{Leva} - h = 0.07$
Shank			0.045	0.36	0.43	$L_{Leva} - h = 0.07$
Foot	0.24	0.08	-	0.06	0.26	$L_{Leva} - l = 0.02$

A maximum difference of 0.23 m is observed when comparing the trunk’s segment lengths of Leva and Frigo et al. This is because Leva’s model combines the length of

the trunk with that of the pelvis. The pelvis segment length ($h_{\text{pelvis}})_{\text{Frigo}}$ can be added to the trunk's ($h_{\text{trunk}})_{\text{Frigo}}$ and the sum ($h_{\text{pelvis}} + h_{\text{trunk}})_{\text{Frigo}}$ has only a difference of 0.07 m when compared with the model of Leva. The total body weight of the two models differ by 0.14 m and the current differences in the combined lengths of head, trunk, thigh, shank and foot height account for that.

3.4.2 Inertia of body segments

Inertia values have been calculated for Winter's model and shown in **Table 7** using the equation shown below.

$$I_p = m \times (l \times R_p)^2 \quad (1)$$

Where m and l are the mass and length of the segment respectively. R_p is the ratio of radius of gyration for the proximal axis to the length of the segment.

Table 7 Calculation of inertia about the proximal axis for Winter's model.

Segments	Length (l) [m]	Mass (m) [kg]	Ratio of radius of gyration about the proximal end to the segment length (R_p)	Inertia about Proximal end (I_p) [kg.m ²]
Head	0.23	5.67	0.12	0.00
Arm	0.32	1.96	0.54	0.06
Forearm	0.25	1.12	0.53	0.02
Hand	0.19	0.42	0.59	0.01
Trunk (THN)	0.50	40.46	0.83	7.01
Thigh	0.43	7.00	0.54	0.37
Shank	0.43	3.26	0.53	0.17
Foot	0.26	1.02	0.69	0.03

The radius of gyration was not given for trunk, but for the combination of trunk, head and neck (THN) or head, arm and trunk (HAT). The former is chosen for calculation of inertia in the table above. Due to the aforementioned reason, the value of Inertia, about the proximal axis, is higher than that of Leva's or Wang's.

The anthropometric data given by Leva has been shown in **Table 8** and were calculated from the radii of gyration percentages with the following formula:

$$I = (M \cdot \bar{m}) \cdot (l \cdot \bar{r})^2 \quad (2)$$

In which M is the total body mass of 73 kgs, \bar{m} is the mean relative mass of the segment, l is the measured length of the segment and \bar{r} is the mean relative radius of gyration of the segment for the specific axis.

Table 8 Anthropometric data for masculine subject, of height 1.741 m and 73 kg, used by de Leva. The Centre of Mass is in the X direction: in local coordinate of the body.

Segment	Mass [% of 73 kg]	Radii of gyration sagittal (Z) [%]	Radii of gyration transverse (X) [%]	Radii of gyration longitudinal (Y) [%]	Length [m]	COM (from proximal) [%]	Segment Mass [kg]
Head	6.94	31.20	36.20	37.60	0.20	0.60	5.07
Arm	2.71	15.80	28.50	26.90	0.28	0.58	1.98
Forearm	1.62	12.10	27.60	26.50	0.27	0.46	1.18
Hand	0.61	40.10	62.80	51.30	0.09	0.79	0.45
Trunk	43.46	19.10	37.20	34.70	0.53	0.45	31.73
Thigh	14.16	14.90	32.90	32.90	0.42	0.41	10.34
Shank	4.33	10.30	25.50	24.90	0.43	0.45	3.16
Foot	1.37	0.12	0.25	0.25	0.26	0.44	1.00

In **Table 9**, the values of inertia for Wang’s model and Leva’s model are compared. The notations I_{33} , I_{11} and I_{22} are used by Wang to denote the inertia values in the sagittal, transverse, and longitudinal directions respectively.

Table 9 Comparison of Inertia values, of the models’ body segments, between Wang and Leva. Inertia values of hip and shoulders are included in the body of the trunk for Leva’s model.

Rigid body	Inertia values of Wang’s model (Weight : 70 kg and Height: 1.8m)			Inertia values of Leva’s model (Weight : 73kg & Height: 1.741m)		
	I_{33} [kg·m ²]	I_{11} [kg·m ²]	I_{22} [kg·m ²]	Sagittal (I_z) [kg·m ²]	Transverse (I_x) [kg·m ²]	Longitudinal (I_y) [kg·m ²]
Head	0.02	0.02	0.03	0.02	0.03	0.03
Arm	0.00	0.01	0.01	0.00	0.01	0.01
Forearm	0.00	0.00	0.00	0.00	0.01	0.01
Hand	0.00	0.00	0.00	0.00	0.00	0.00
Trunk	0.22	0.36	0.28	0.33	1.24	1.08
Thigh	0.03	0.12	0.12	0.04	0.20	0.20
Shank	0.00	0.04	0.04	0.01	0.04	0.04
Foot	0.00	0.00	0.00	0.00	0.00	0.00

In de Leva’s and Wang’s model data, the value of mass percentage of the trunk had a difference of 15.27%. The inertias are different by more than a value of 0.01 kg·m² for the head, trunk, and thigh.

3.5 Mechanical model definition in Newton Dynamics Engine

After the model data is imported from the xml, using the methods offered by TinyXML library, the next step is to create the segments individually by creating a new ‘GeomNewton’ object and setting the body type as dynamic in nature.

The creation of two segments (segment 1 and 2), the joints and the methods used to join the segments at the joint have been described to serve as an example.

Segment 1

The first segment, S1, is created as a GeomNewton object and the body type is set as 'Dynamic'.

```
// create segment 1
S1 = new GeomNewton(m_winManager->aManager);
S1->SetBodyType(adtDynamic);
```

The texture from default ones in the library is set and color is set by giving the RGB values as input for the segment.

```
S1->SetTexture0(&tex[0], "Tex0");
S1->SetDiffuseColor(0.7f, 0.7f, 0.7f);
```

The initial alignment of the segment 1 is set by defining the angle of orientation and the position

```
S1->SetRollAngle(90.0f, false);
S1->SetPosition(_Pos.x, _Pos.y, _Pos.z);
```

With the values of segment 1 length and the radius of bones, the segment 1 is created inside the Newton engine as 'Capsule' type geometry. The fourth input, given to InitNewton below, is the mass of the segment.

```
S1->InitNewton(atCapsule, radius, radius, length, 10.0f);
```

The NewtonBody type object is queried from the GeomNewton object created in the earlier steps and is passed as an input to 'NewtonBodySetTransformCallback' method. This allows to set and update the transformation matrix on the segment later on in the code.

```
m_body = S1->GetBody();
NewtonBodySetTransformCallback(m_body, NULL);
```

Segment 2

Now that segment 1 is created, S2 can also be created in a similar way.

```
// create Spine segment
S2 = new GeomNewton(m_winManager->aManager);
S2 ->SetBodyType(adtDynamic);
```

The previously created S1 is set as the parent for S2 before initializing the object in Newton.

```
S2 ->SetParent(S1);
S2 ->SetTexture0(&tex[0], "Tex0");
S2 ->SetDiffuseColor(1.0f, 1.0f, 1.0f);
S2 ->SetPosition(0, ( l_S1 + l_S2) / 2 + 2 * r_bones, 0);
S2 ->InitNewton(atCapsule, r_bones, r_bones, l_S2, 10.0f);
NewtonBodySetTransformCallback(S2 ->GetBody(), NULL);
```

A joint node object of S2 is created which can be used later as reference for constructing new segments or tracking the position of the joint region. The mass and inertia values in the three axes are set for S2.

```
Joint_Node = new dModelNode(S2->GetBody(), dGetIdentityMatrix(), this);
NewtonBodySetMassMatrix(S2->GetBody(), mass_S2, Ixx_S2 , Iyy_S2 , Izz_S2 );
```

The center of mass of the body is offset to the value in literature.

```
dVector com;
NewtonBodyGetCentreOfMass(S2->GetBody(), &com[0] );
com.m_y += DeltaCM_S2;
NewtonBodySetCentreOfMass(S2->GetBody(), &com[0]);
```

Joint

Now that the segments 1 and 2 are created, they are ready to be joined by a joint. The angle in which the joint will be aligned and the position with reference to the point connecting S1 and S2 are set.

```
// create Lumbar joint.
dMatrix S2_PinMatrix(dYawMatrix(90.0f * dDegreeToRad));
S2_PinMatrix.m_posit = dVector(_Pos.x , _Pos.y + l_S1/2 + r_bones, _Pos.z);
```

With the rotation and translation matrix created above and the body objects of the segments 1 and 2, the joint is created as a 'dCustomDoubleHinge' and the stiffness and damping values are set. The method 'SetMassIndependentSpringDamper' takes as input the state, relaxation distance of 0.3, the joint stiffness value of 10^6 N/m and damping value of 10^4 Ns/m.

```
Joint = new dCustomDoubleHinge(S2_PinMatrix, S2->GetBody(), S1->GetBody());
Joint ->SetMassIndependentSpringDamper(true,0.3, 1.e6f, 1.e4f);
Joint ->SetMassIndependentSpringDamper1(true,0.3, 1.e6f, 1.e4f);
```

The joints are pushed back into a vector containing the list of joints. This helps when iterating through and updating the position in every frame.

```
m_winManager->aManager->vJointList.push_back(Disk2);
```

With the same procedure, described above, all the other joints and segments can be created.

The sacrum is defined as the first or root parent, the parent child relationships among the subsequent segments follow the pattern shown in **Figure 15** below.

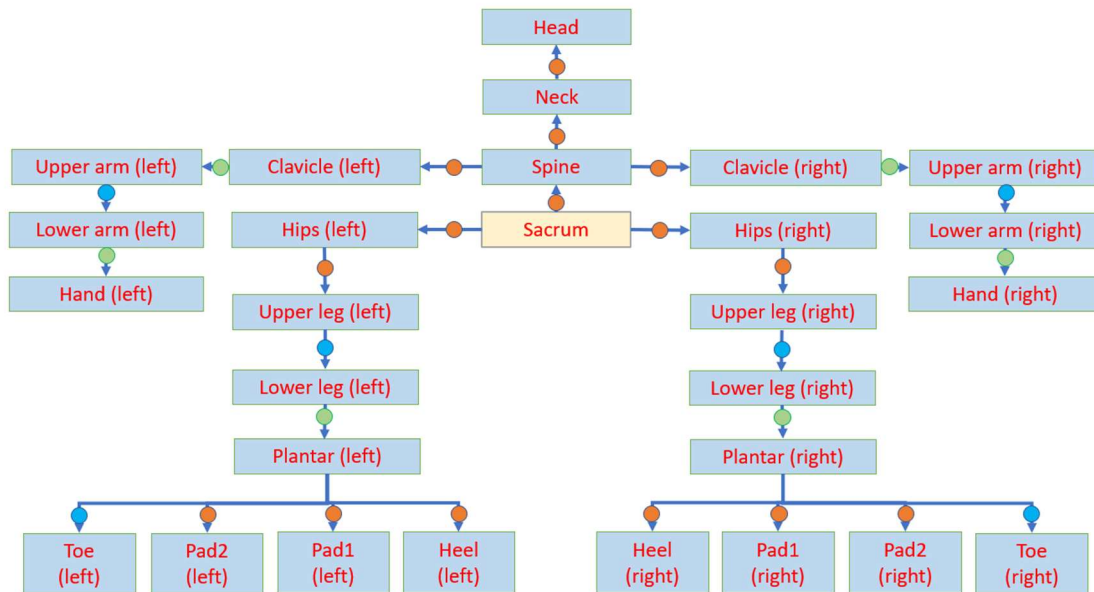


Figure 15 Parent child hierarchy of the segments. The sacrum is the root parent. The orange dots represent double hinge joint, the green ones represent ball and socket joints, and the blue ones indicate hinge joints. There are 15 unique joints which makes a total of 27 joints when counting both the left and right sides.

The method `GetPosition()` when called on a segment's `GeomNewton` object, retrieves its position vector. Its usage has been shown in **Table 11**. In the above figure, the orange dots represent double hinge joint, the green ones represent ball and socket joints, and the blue ones indicate hinge joints. There are 15 unique joints (9 double hinge joints, 3 ball and socket joints and 3 hinge joints) which makes a total of 27 joints when counting both the left and right sides. The three types of joints and their axes of rotations are described in **Figure 16** below.

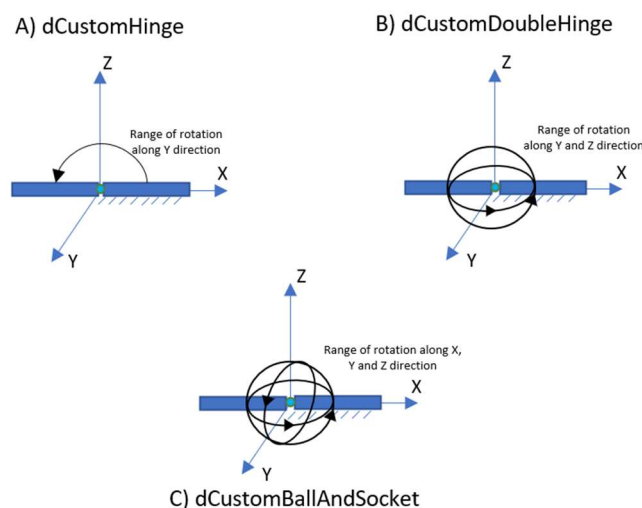


Figure 16 The three joint class types used to connect the body segments: A) `dCustomHinge` allows motion only along one axis; B) `dCustomDoubleHinge` allows rotation in 2 axes; C) `dCustomBallAndSocket` joint allows rotation along all the three axes

The segments are created this way and the only step remaining in order to create the complete skeletal model is to define the joints connecting these segments. The joint class types attaching the body segments are pointed out in **Figure 15**. Limits have been set on the knee, elbow and hip joints, during their creation, to prevent biologically unrealistic angles of the segments with respect to each other. These constraints have been described in **Table 10**.

Table 10 Constraints set on elbows, hip joints and knees. As the hip joint is double hinge, rotation is allowed in the lateral direction

Joint	Connecting Segments	Angle range in frontal direction [°]	Angle range in lateral direction [°]
Elbow	Upper arm – Lower arm	0 to 180	-
Hip joint	Upper leg - Hip	-40 to 120	-30 to 5
Knee	Lower leg – Upper leg	-180 to 0	-

The hip joint connecting the hip and the upper leg is a double hinge in which the bending direction in lateral plane is also constrained as shown in the above table.

The details of the muscle classes that actuate the body segments, previously defined, have been discussed in the following section.

Table 11 Parent, Child segments with the joints connecting them. *_Pos* is the initial position of the human model, it is given by the coordinates ($X = 0$, $Y = l_Sacrum/2 + l_Up_Leg + l_Low_Leg + h_foot + l_Hip + 0.25f$, $Z = 0$), $r_bones = 0.07m$ is the radius of the bones.

Segment (Parent)	Joint 1	Segment 2 (Child)	Joint Rotation (°)			Joint Position		
			Pitch	Roll	Yaw	X	Y	Z
Sacrum	Lumbar Joint	Spine	-	-	90	$_Pos.x$	$_Pos.y + l_Sacrum / 2 + r_bones$	$_Pos.z$
Spine	Neck Joint	Neck	-	-	-	$Neck \rightarrow GetPosition().m_x$	$Neck \rightarrow GetPosition().m_y$	$Neck \rightarrow GetPosition().m_z$
Neck	Head Joint	Head	-	-	90	$Head \rightarrow GetPosition().m_x$	$Head \rightarrow GetPosition().m_y$	$Head \rightarrow GetPosition().m_z$
Sacrum	Sacrum Joint (L/R)	Hip (L/R)	-	-	90	$_Pos.x + r_bones$	$_Pos.y - l_Sacrum / 2$	$_Pos.z$
Hip (L/R)	Hip Joint (L/R)	Upper Leg (L/R)	90	-	-	$Up_Leg_L \rightarrow GetPosition().m_x$	$Up_Leg_L \rightarrow GetPosition().m_y + l_Up_Leg / 2$	$Up_Leg_L \rightarrow GetPosition().m_z$
Upper Leg (L/R)	Knee Joint (L/R)	Lower Leg (L/R)	90	-	-	$Low_Leg_L \rightarrow GetPosition().m_x$	$Low_Leg_L \rightarrow GetPosition().m_y + l_Low_Leg / 2$	$Low_Leg_L \rightarrow GetPosition().m_z$
Lower Leg (L/R)	Ankle Joint (L/R)	Plantar (L/R)	-	90	-	$Low_Leg_L \rightarrow GetPosition().m_x$	$Low_Leg_L \rightarrow GetPosition().m_y - l_Low_Leg / 2 - r_bones$	$Low_Leg_L \rightarrow GetPosition().m_z$
Spine	Sternum Joint	Clavicle (L/R)	-	-	90	$Spine \rightarrow GetPosition().m_x + r_bones$	$Spine \rightarrow GetPosition().m_y + l_Spine / 2$	$Spine \rightarrow GetPosition().m_z$
Clavicle (L/R)	Shoulder Joint	Upper Arm (L/R)	-	-	90	$Up_Arm_L \rightarrow GetPosition().m_x$	$Up_Arm_L \rightarrow GetPosition().m_y + l_Up_Arm / 2$	$Up_Arm_L \rightarrow GetPosition().m_z$
Upper Arm (L/R)	Elbow Joint	Lower Arm (L/R)	90	-	-	$Low_Arm_L \rightarrow GetPosition().m_x$	$Low_Arm_L \rightarrow GetPosition().m_y + l_Low_Arm / 2$	$Low_Arm_L \rightarrow GetPosition().m_z$
Lower Arm (L/R)	Wrist Joint	Hand (L/R)	-	-	90	$Hand_L \rightarrow GetPosition().m_x$	$Hand_L \rightarrow GetPosition().m_y + l_Hand / 2$	$Hand_L \rightarrow GetPosition().m_z$
Plantar (L/R)	Heel Joint (L/R)	Heel (L/R)	-	-	-	0	$- h_sphere$	$(l_plantar / 2)$
Plantar (L/R)	Pad1 Joint (L/R)	Pad1 (L/R)	-	-	-	$w_foot / 2$	$- h_sphere$	$- (l_plantar / 4)$
Plantar (L/R)	Pad2 Joint (L/R)	Pad2 (L/R)	-	-	-	$- w_foot / 2$	$- h_sphere$	$- (l_plantar / 4)$
Plantar (L/R)	Toe Flexing Joint (L/R)	Toe (L/R)	90	-	-	$Plantar_L \rightarrow GetPosition().m_x$	$Plantar_L \rightarrow GetPosition().m_y$	$Plantar_L \rightarrow GetPosition().m_z - l_plantar / 2$

3.6 Lower limbs activation

In this section, the muscular activation of the lower limbs is described. Different walking models are actuated by Hill's muscles [13, 38] to model the mechanical behavior of the sarcomeres, muscle fibers and tendon. Also in this thesis work, a Hill-type muscle model has been used to compute the force needed to actuate the legs of the model.

3.6.1 Muscle force based on Newton-Raphson algorithm

For the Hill-type muscle model represented in **Figure 17**, l_{CE} is considered as the internal state variable to perform Newton-Raphson algorithm.

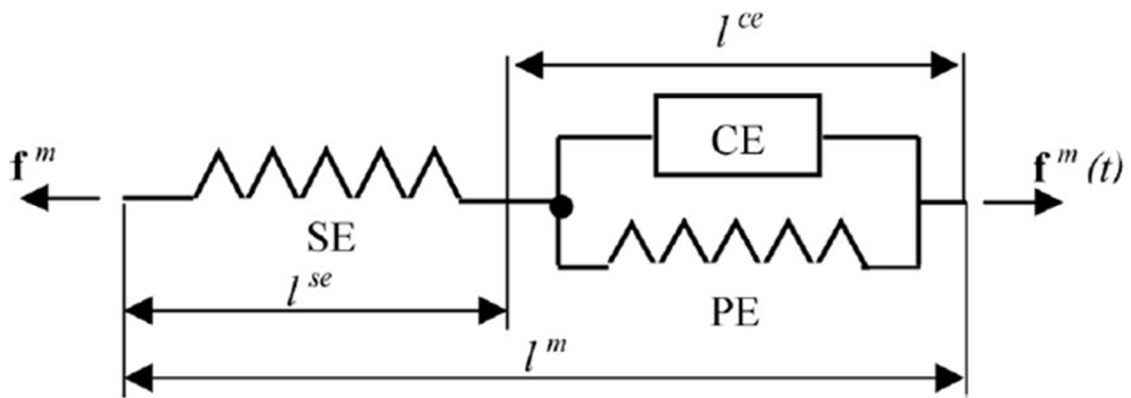


Figure 17 Hill-type muscle model showing the lengths l_{CE} , l_{SE} and l_m , and of the contractile element, serial element and entire musculotendon unit respectively. $f^m(t)$ is the force exerted by the entire muscle unit at a time t .

At each time step, the increment of length of the contractile element (Δl_{CE}) is computed following the procedure shown in this section.

$$F_{CE} \left(l_{CE} + \Delta l_{CE}, \frac{d(l_{CE} + \Delta l_{CE})}{dt} \right) = F_{CE} \left(l_{CE} + \Delta l_{CE}, \frac{\Delta l_{CE}}{\Delta t} \right) \quad (3)$$

Where F_{CE} is the force exerted by the contractile element. We use \tilde{l} which is the normalized length of the contractile element to check if the contractile element is over extended or over contracted.

$$\tilde{l} = (l_{CE} + \Delta l_{CE}) / l_{opt} \quad (4)$$

Where l_{opt} is the optimum length of the muscle obtained from literature.

To calculate the components of force exerted by higher and lower parallel elements:

$$f_{HPE} = \left(\frac{\tilde{l} - 1.0}{0.56} \right)^2, \text{ if } \tilde{l} > 1 \text{ (over-extension)} \quad (5)$$

$$f_{LPE} = \left(\frac{0.44 - \tilde{l}}{0.28} \right)^2, \text{ if } \tilde{l} < 0.44 \text{ (over-contraction)} \quad (6)$$

$$F_{PE}(l_{CE} + \Delta l_{CE}) = F_0(f_{HPE} - f_{LPE}) \quad (7)$$

Where F_{PE} is the resulting force exerted by the parallel element and F_0 is the maximum muscle force of the specific muscle group.

For the calculation of resultant force exerted by the serial element (F_{SE}) the normalized length of the serial element (\tilde{l}_s) is calculated.

$$\tilde{l}_s = \frac{d - (l_{CE} + \Delta l_{CE})}{l_{opt}} \quad (8)$$

Where d is the current distance between the origin and insertion points of the muscle group.

$$F_{SE}(l_{CE} + \Delta l_{CE}) = F_0 \left(\frac{\tilde{l}_s - 1}{0.04} \right)^2 \quad (9)$$

F_{PE} & F_{SE} are a function of total length of the contractile element ($l_{CE} + \Delta l_{CE}$). The error function $Err(\Delta l_{CE})$ is calculated as shown below:

$$Err(\Delta l_{CE}) = F_{CE} + F_{PE} - F_{SE} \quad (10)$$

The exact derivatives, with respect to change in length of the contractile element, of forces of

$$\text{Contractile element: } \frac{dF_{CE}}{d\Delta l_{CE}} \left(l_{CE} + \Delta l_{CE}, \frac{\Delta l_{CE}}{\Delta t} \right),$$

$$\text{Parallel element: } \frac{dF_{PE}}{d\Delta l_{CE}} (l_{CE} + \Delta l_{CE}) \text{ and}$$

$$\text{Serial element: } \frac{dF_{SE}}{d\Delta l_{CE}} (l_{CE} + \Delta l_{CE})$$

are used to calculate the derivative of the previously calculated error function with respect to the change in length of the contractile element as shown below:

$$\frac{dErr(\Delta l_{CE})}{d\Delta l_{CE}} = \frac{dF_{CE}}{d\Delta l_{CE}} + \frac{dF_{PE}}{d\Delta l_{CE}} - \frac{dF_{SE}}{d\Delta l_{CE}} \quad (11)$$

The change in the length of contractile element Δl_{CE} is calculated using the equation below:

$$\Delta l_{CE} = \Delta l_{CE} - \frac{Err(\Delta l_{CE})}{\frac{dErr(\Delta l_{CE})}{d\Delta l_{CE}}} \quad (12)$$

This way the value of Δl_{CE} is calculated for every time step and updated. A tolerance value of 10^{-3} is fixed and when

$$Err(\Delta l_{CE}) > Tolerance \quad (13)$$

The iteration is stopped. This means that the sum of the forces of contractile element and the parallel element is equal to that of the serial element.

$$F_{CE} + F_{PE} \approx F_{SE} \quad (14)$$

3.6.2 Muscle force computation by solving the inner degree of freedom of Hill-type Musculotendon Unit

One of the ways to define a walking human model is to develop a two legged spring mass model as demonstrated by Geyer and Herr [38]. Here, motion of the body is simplified into a point mass travelling on two massless spring legs. To transform the aforementioned model into a neuromuscular one, that is more realistic, involves a three-step process: the spring legs are replaced with segments whose stance behaviour are generated by extensor muscles at the knee and the ankle, then the oscillating point mass is replaced with a trunk that should be supported by hip muscles to keep it upright and finally, the legs should be swung in order to enter a cyclic walking motion.

The skeletal segment model used in this study are actuated by eight hill type muscles. In this thesis, the model of the muscle is the one proposed by Geyer (see **Figure 18**) and the force generated by each MTU is the sum of the force contributed by a Contractile Element (CE), Series Element (SE) and two Parallel Elements, Higher and Lower (HPE and LPE). The SE gives the contribution of the tendon, while the sum of the contributions of HPE and LPE gives the passive forces generated by the muscle fibers (F^{PE}). The force of the musculotendon unit is expressed as:

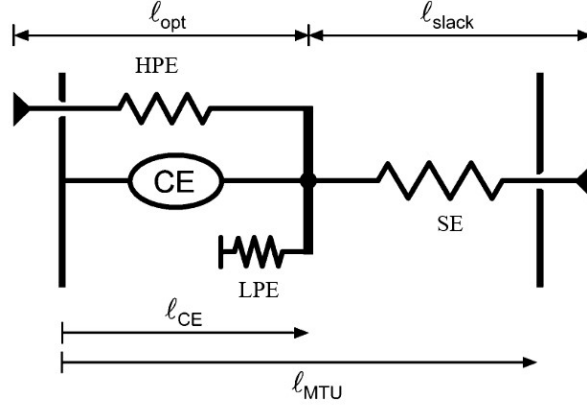


Figure 18 Type Hill's muscle with contractile element (CE), higher parallel elasticity (HPE), lower parallel elasticity (LPE) and series elasticity (SE).

$$F^{MTU} = F^{CE} + F^{PE}, \quad (15)$$

which individually can be expressed as

$$F^{CE} = aF^0 f_l(\tilde{l}^{CE}) f_v(\tilde{v}^{CE}), \quad (16)$$

$$F^{PE} = F^{HPE} - F^{LPE}. \quad (17)$$

F^{CE} is a function of the actuation level a , the maximum force that the muscle can exert F^0 , the length of the contractile element $f_l(\tilde{l}^{CE})$ and its contraction velocity $f_v(\tilde{v}^{CE})$. a is a value between 0 and 1 and is a function of the neural actuation and will be described in the following chapter. F^0 is the maximum isometric force that depends on the actuated muscle and is derived from literature. f_l is the muscle length contribution and is expressed by the following formula:

$$f_l(\tilde{l}^{CE}) = \exp\left(\ln(0.05) \left(0.56^{-1}(\tilde{l}^{CE} - 1)\right)^4\right). \quad (18)$$

\tilde{l}^{CE} is the length of the contractile element normalized by its optimal length l_{opt} , defined when the muscle can exert the maximum force F^0 . In detail:

$$\tilde{l}^{CE} = \frac{l_{CE}}{l_{opt}}. \quad (19)$$

$f_v(\tilde{v}^{CE})$ is expressed by two different formulas, depending on whether the muscle flexes (Hill's formula) or extends (Aubert's formula):

$$f_v(\tilde{v}^{CE}) = \begin{cases} \frac{-v^m - \tilde{v}^{CE}}{-v^m + 5\tilde{v}^{CE}}, & \text{if } \tilde{v}^{CE} < 0 \\ 1.5 + 0.5 \frac{-v^m + \tilde{v}^{CE}}{37.8\tilde{v}^{CE} + v^m}, & \text{if } \tilde{v}^{CE} \geq 0 \end{cases}, \quad (20)$$

where v^m is the maximum contraction velocity of the muscle derived by literature and \tilde{v}^{CE} is the contraction velocity on the contractile element normalized by l_{opt} , in detail:

$$\tilde{v}^{CE} = \frac{v_{CE}}{l_{opt}}. \quad (21)$$

The force parallel to the contractile element is the sum of the contribution of the Lower Parallel Element (LPE), that prevents the CE contracting below reasonable limit, and the higher parallel element (HPE) that is the equivalent stiffness of the muscle. In detail:

$$F^{HPE} = F^0 \left(0,56^{-1} (\tilde{l}^{CE} - 1) \right)^2 \text{ if } l_{CE} > 0,44 l_{opt}, \quad (22)$$

$$F^{LPE} = F^0 \left(0,28^{-1} (0,44 - \tilde{l}^{CE}) \right)^2 \text{ if } l_{CE} < l_{opt}. \quad (23)$$

Thanks to force equilibrium, it is possible to write:

$$F^{MTU} = F^{CE} + F^{PE} = F^{SE}, \quad (24)$$

where F^{SE} is the force exerted by the tendon modelled by the element in series (SE) with the contractile element. Its expression is:

$$F^{SE} = F^0 \left(0,04^{-1} (\tilde{l}^{SE}) \right)^2 \text{ if } l_{SE} > l_{slack}, \quad (25)$$

where \tilde{l}^{SE} is the length of the series element normalized by slack length of the tendon (l_{slack}), derived from literature. In detail:

$$\tilde{l}^{SE} = \frac{l_{SE}}{l_{slack}}, \text{ where } l_{SE} = l_{MTU} - l_{CE} \quad (26)$$

SE exerts a force if its length is higher than the slack length of the tendon, else no force is generated by SE. Also, F^{LPE} is different from zero if the CE contracts to a length below 44% of l_{opt} . Finally, F^{HPE} is different from zero if l_{CE} is bigger than l_{opt} .

For a given muscle, the length is defined as:

$$l^{MTU} = l^{opt} + l^{slack} + \sum_{j \in J} \Delta^i(\theta), \quad (27)$$

where J is the set of joints attached to the muscle, θ is the joint angle and Δ^i expresses the length variation of the muscle according to joint angles.

For the hip:

$$\Delta^i(\theta) = \rho r(\theta - \phi^R), \quad (28)$$

while for knee and ankle:

$$\text{Penn: } \Delta^i(\theta) = \rho r(\sin(\theta - \phi^R) - \sin(\phi^R - \phi^M)). \quad (29)$$

Where ρ accounts for the pennation angles, ϕ^M is defined as the joint angle with the maximum moment arm and ϕ^R is the joint angle without length variation ($\Delta^i = 0$). Since l^{MTU} is completely defined by the geometry of the muscle model, l^{CE} is the only quantity to be computed.

In the next sections, two different actuation methods to solve the inner degree of freedom of the type Hill's model are presented: 1) to compute the torque of the muscle generated at the actuated joint. 2) To compute the force produced by the muscle by an iterative method and applied to the insertion and origin points of linked bodies.

The inner degree of freedom of the type Hill's muscle model is solved by the numeric integration of the actual velocity. In fact, given the geometry of the muscle, it is possible to express the velocity formula by inverting Eq. 8. Then, the value of the length of the contractile element is calculated by finding the product of its current velocity (v^{CE}) with the time step (Δt)

$$l^{CE} = v^{CE} * \Delta t \quad (30)$$

Thus, the force of the muscle can be computed according to Eq. 12 and the corresponding torque can be computed according to:

$$T_m = r_0 * F_{MTU} \quad (31)$$

Where r_0 is the arm of muscle given in the next section.

3.6.3 Properties of muscle in literature

The eight Hill-type muscles should be inserted at proper locations with respect to the body segments. The origin and insertion points are always measured from the upper end of the corresponding segment. A maximum isometric force is set for each of the 8 muscle groups used. By our model, this is the force exerted by the muscle, in its axial direction, when it is at its maximum capacity.

In **Table 12**, the maximum force, maximum velocity, optimal length and the slack length used by Geyer and Herr (Yamaguchi et al [41]) have been described.

Table 12 MTU parameters values are estimated from Yamaguchi et al assuming a force of 25 N per cm² cross sectional area, maximum velocity of 6 for slow and 12 for medium-fast twitch muscles, and l_{opt} , l_{slack} values to reflect muscle fiber, tendon lengths

Muscle group	Maximum force [N]	Maximum velocity [l_{opt}/s]	l_{opt} [cm]	l_{slack} [cm]
SOL	4000	6	4	26
TA	800	12	6	24
GAS	1500	12	5	40
VAS	6000	12	8	23
HAM	3000	12	10	31
RF	1000	12	8	28
GLU	1500	12	11	13
HFL	2000	12	11	10

In **Table 13** , the attachment parameters of muscle groups used by Geyer and Herr have been shown.

Table 13 MTU attachment parameters used by Geyer and Herr. Arm length (r_0), ϕ_{ref} is the reference joint angle at which $l_{mtu} = l_{opt} + l_{slack}$, lever length, $r_m(\phi) = r_0 \cdot \cos(\phi - \phi_{max})$ for the ankle and the knee while $r_m(\phi) = r_0$ for the hip. ρ accounts for the for muscle pennation angles and ensures that the MTU fiber length stays within the physiological limits throughout the joint work space. Change in the MTU length $\Delta l_{mtu} = \rho r(\phi - \phi_{ref})$ for the hip and $\Delta l_{mtu} = \rho r[\sin(\phi - \phi_{max}) - \sin(\phi_{ref} - \phi_{max})]$ for the angle and knee

Joints	Muscle group	r_0 [cm]	ϕ_{max} (deg)	ϕ_{ref} (deg)	ρ
ankle	SOL	5	110	80	0.5
	TA	4	80	110	0.7
	GAS	5	110	80	0.7
knee	GAS	5	140	165	0.7
	VAS	6	165	125	0.7
	HAM	5	180	180	0.7
hip	HAM	8	-	155	0.7
	GLU	10	-	150	0.5
	HFL	10	-	180	0.5

Reiner and Fuhr developed a three segmental model with nine mono and biarticular muscle groups whose schematic is shown in **Figure 19** [42].

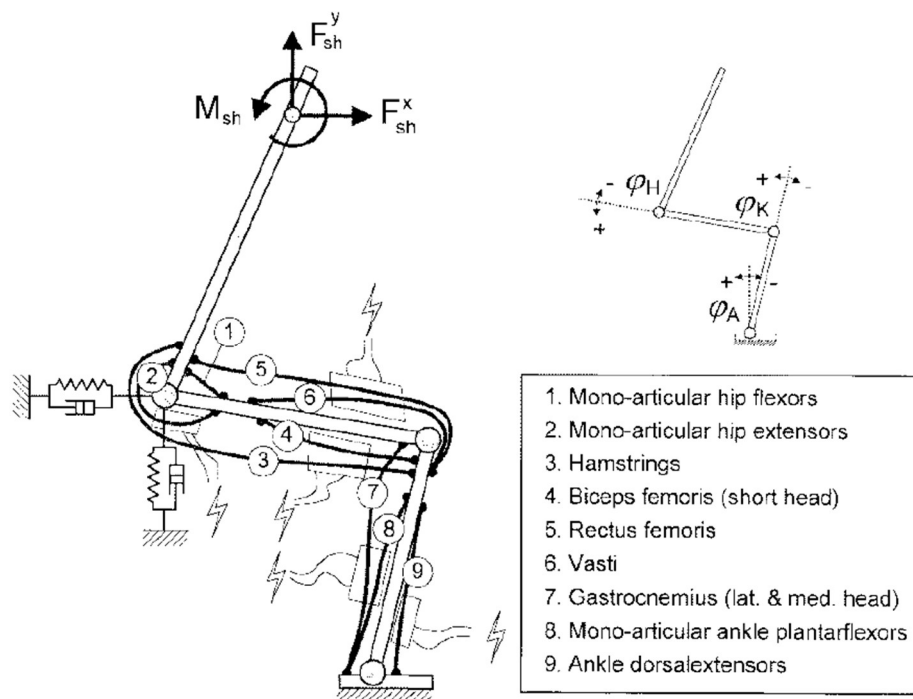


Figure 19 Nine muscle group model developed by Reiner and Fuhr. The spring damper system represents forces involved in body seat interaction. The two forces and one moment at the shoulder represent the control actions of the neurologically intact upper body. The values of ϕ_H , ϕ_K and ϕ_A represent the angles at the hip, knee and ankle respectively. Source: IEEE Transactions on Rehabilitation Engineering, 6(2), 113–124. <https://doi.org/10.1109/86.681177>

In **Table 14**, the muscle properties like maximum force, optimal length and maximum velocity of Reiner and Fuhr's model have been shown.

Table 14 Muscle groups and their corresponding maximum isometric force (F_{max}), optimal muscle length (l_{opt}) and maximum contraction velocity (V_{max}) as described by Reiner and Fuhr

No	Muscle Group	Symbol	F_{max} [N]	l_{opt} [m]	V_{max} [m/s]
1	Mono-articular hip flexors	HFL	1850	0.15	0.73
2	Mono-articular hip extensors	GLU	2370	0.11	0.54
3	Hamstrings	HAM	2190	0.12	0.48
4	Biceps femoris (short head)	BF	400	0.17	0.69
5	Rectus femoris	RF	1000	0.09	0.51
6	Vasti	VAS	5200	0.09	0.48
7	Gastrocnemius (lat. & med. head)	GAS	1600	0.05	0.32
8	Mono-articular ankle plantarflexors	SOL	3600	0.03	0.1
9	Ankle dorsalextensors	TA	1100	0.09	0.36

3.7 Muscle definition in Newton Dynamics Engine

Methods for getting and setting the origin and insertion points for the muscles have been built into the Muscle class. Sixteen instances of the aforementioned class were initialized to represent the sixteen muscle groups whose schematic are as shown in **Figure 4**. To set the nervous excitation at every frame, the method SetExcitation has been used. There is also a method to set the step size associated with the conversion of nervous excitation into muscular activation.

There are also methods to calculate the various components of forces and lengths associated with Series Elements, Contractile Elements, Parallel Elements and also a method called GetForceElas that returns the force applied by that muscle at every frame. This method contains the steps to calculate the change in the length of contractile element by means of Newton-Raphson algorithm whose details are described in the literature review section.

In chapter 4 the anthropometric data and the muscle data mentioned in the current chapter, have been compared and the actuation simulation results have been described.

Chapter 4: data analysis and actuation simulation

4.1 Anthropometric data comparison

On comparing the lengths of body segments used by Winter, Wang and Leva, maximum deviation is seen for the hand. These lengths have been plotted in **Figure 20**.

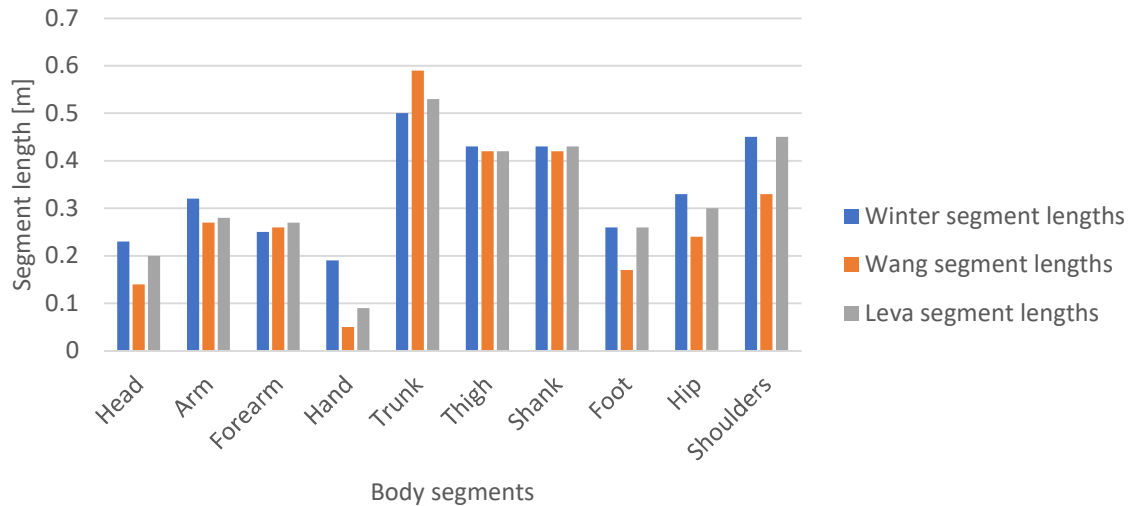


Figure 20 Comparison between body segment lengths given by Winter, Wang and Leva

When comparing the inertia values given, by Wang with that of Leva, in the transverse, longitudinal and sagittal planes, the trunk's inertia given by both the authors can be seen to differ considerably. These differences can be observed in **Figure 21**.

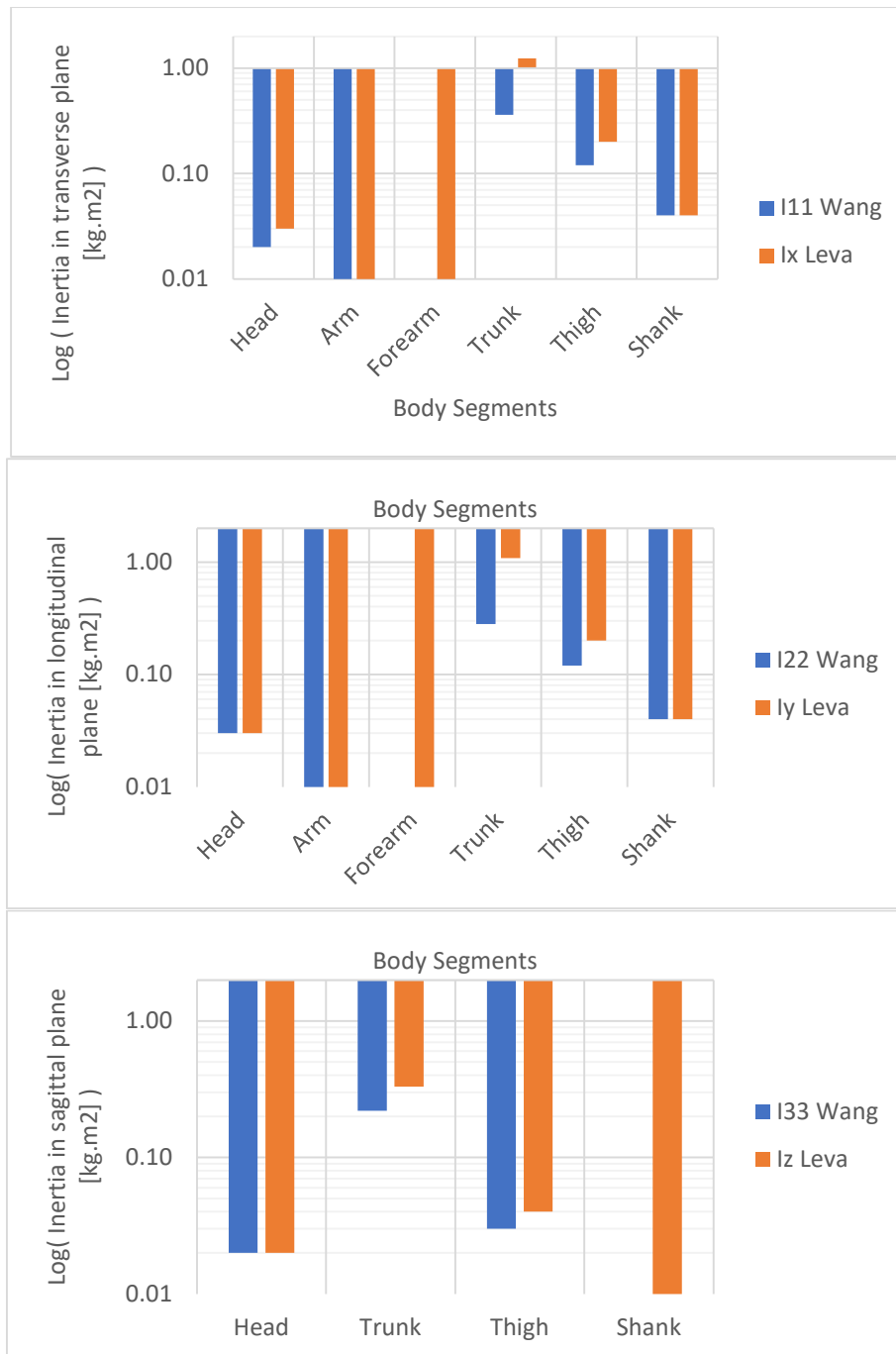


Figure 21 Comparison of Wang and Leva models' logarithmic values of inertia in transverse, longitudinal and sagittal planes for the eight body segments. The maximum difference is observed in the inertia of trunk, for all the three directions.

In **Figure 22**, the mass percentages of the body segments with respect to the total body weight have been compared for the values given by Leva, Wang and Brunner.

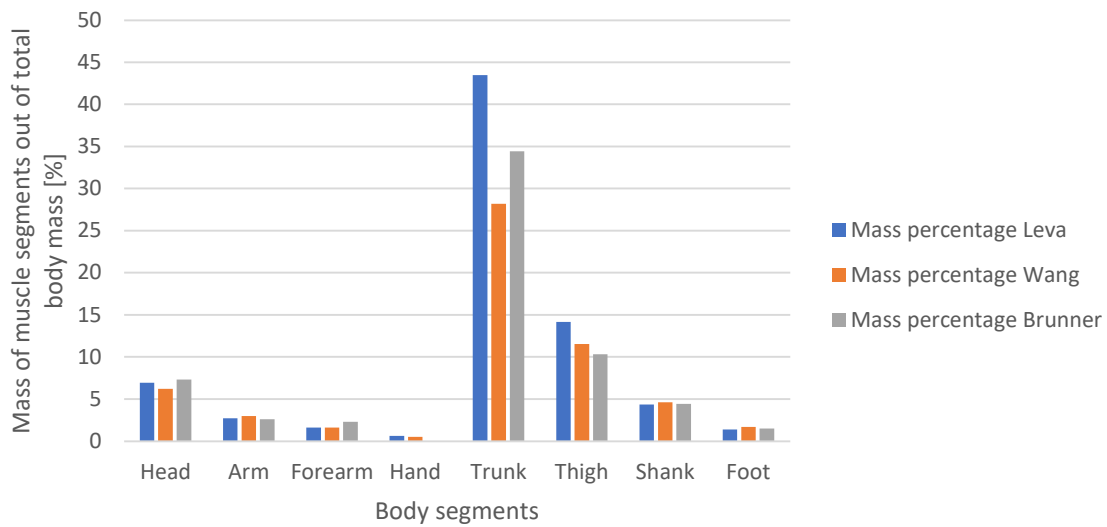


Figure 22 Comparison of mass percentages of segments given by Leva, Wang and Brunner

The mass percentages of the trunk, given by the three authors, have the maximum difference because Leva’s model combines the trunk segment’s mass with that of the pelvis. Also, it is common for the mass distribution of trunk to vary even among subjects of same height. The mass of forearm and hand are combined in the values presented by Brunner, so the model’s hand has no contribution individually.

The body segments along with the joints connecting them are labelled in **Figure 23**.

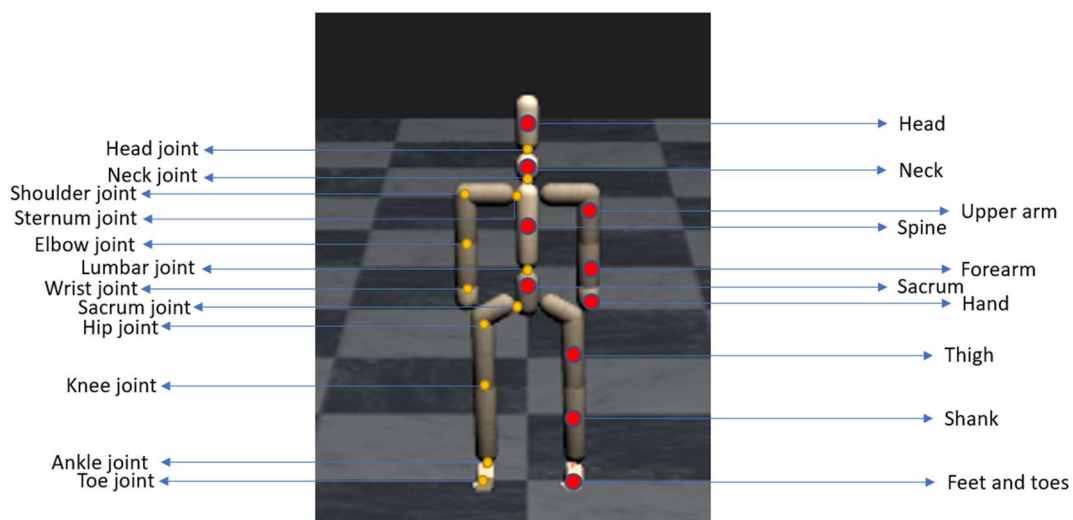


Figure 23 Body segments (red points) and their connecting joints (yellow points) whose data are in table 1

In **Figure 24**, the dimensions and mass distribution have been described.

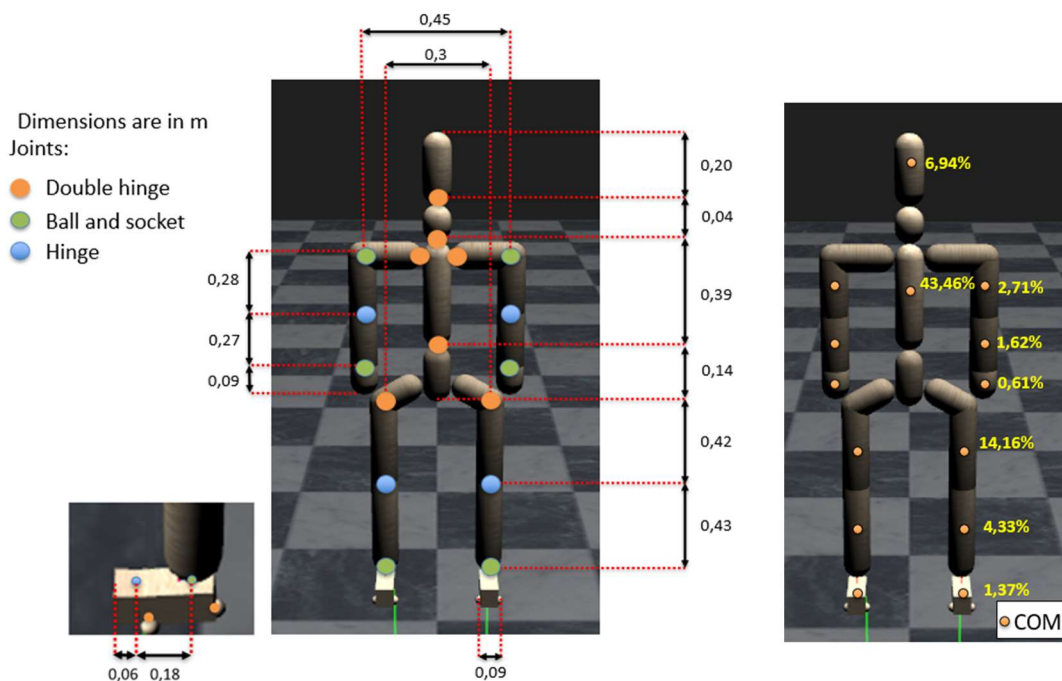


Figure 24 Initial model built in Newton Dynamics engine using the Human model data used by Leva. Lengths (left) and mass distribution (right) for the segments. The model has a total mass of 73 kg and each segment has its mass expressed as % of total mass and is located at its centre of mass (COM)

Since the differences between the anthropometric data presented by Leva and Winter are minor, and Leva's data is widely used in the research conducted in the field of biomechanics, it has been chosen to design the segments of the human body model used in this study. The missing values were computed applying Winter's proportions.

4.2 Muscle data comparison

The differences in the values of maximum muscle force, maximum muscle velocity and optimal length for each muscle group has been described in the bar-charts shown in **Figure 25**, **Figure 26** and **Figure 27** respectively. The muscle groups BF and RF are unique to Reiner's model, so the respective bars are not seen for those groups for Geyer et al [42, 38].

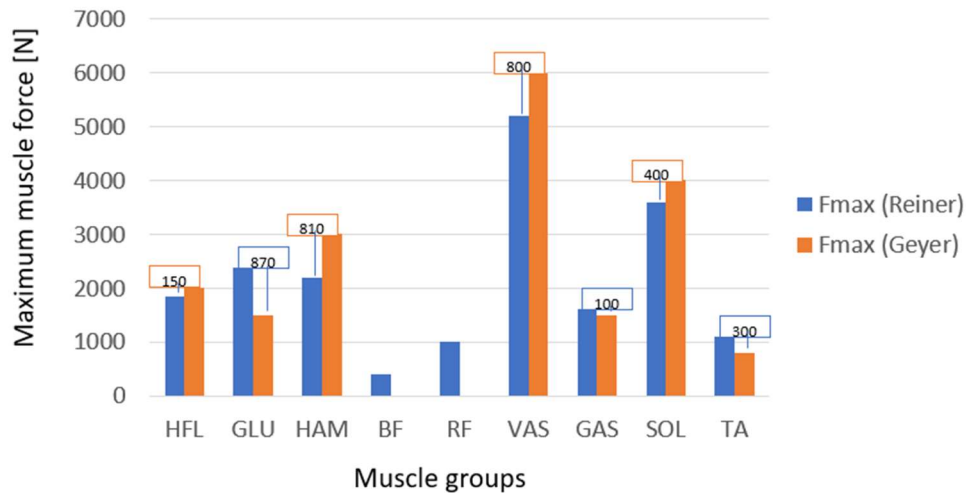


Figure 25 Comparison of Geyer's and Reiner's data for maximum muscle force exerted. The differences in muscle force has been highlighted above each muscle group's bar

A maximum force difference of 870 N is observed for GLU group, while the GAS group differs only by 100 N.

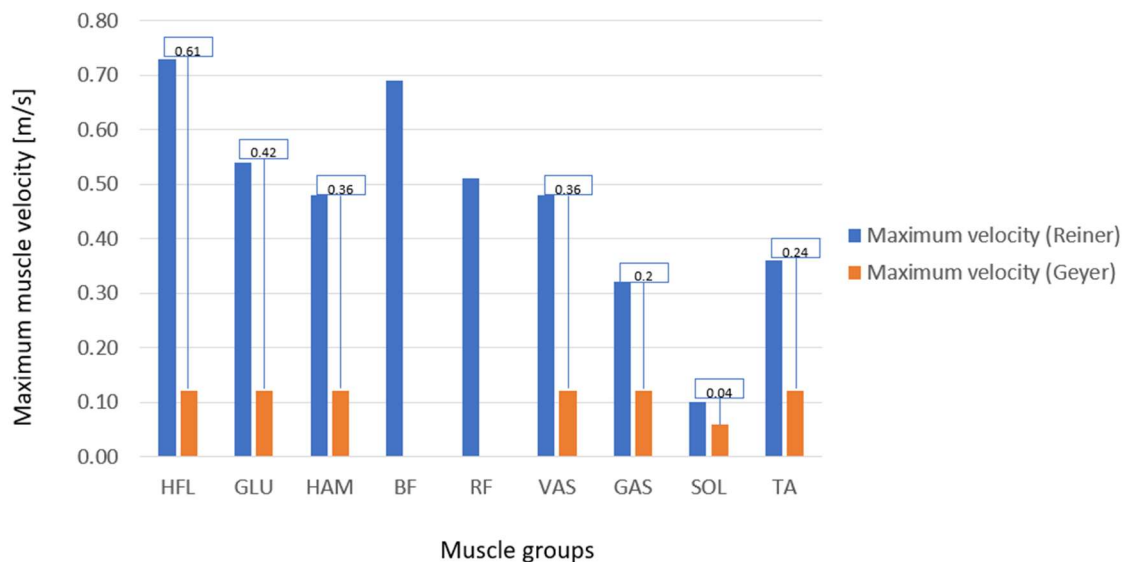


Figure 26 Comparison of Geyer's and Reiner's data for maximum velocities. The differences in maximum muscle velocity has been highlighted above each muscle group's bar

A large difference is observed for all the muscle groups when comparing the values of velocity. A maximum difference of 0.61 m/s is observed for the HFL muscle group while the SOL group varies only by 0.04 m/s.

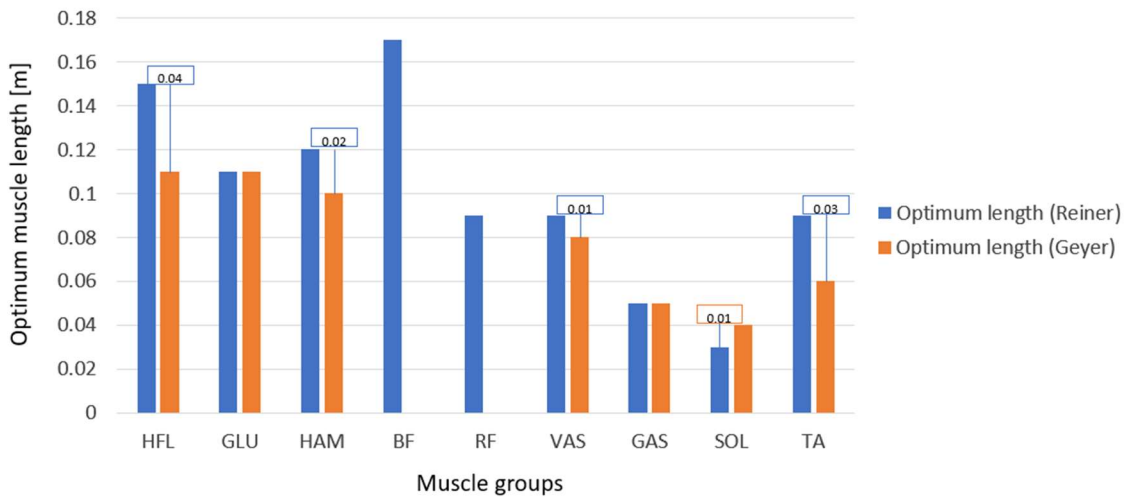


Figure 27 Comparison of Geyer's and Reiner's data for optimum muscle lengths. The differences in optimum muscle lengths has been highlighted above each muscle group's bar

Maximum difference of 0.04 m is observed when comparing Reiner's and Geyer's values of muscle lengths for the HFL group, whereas the GLU group and the GAS group are identical when comparing both the authors' values.

4.3 Experiments on lower limbs activation

The thigh and the shank segment connected by VAS muscle group is provided activation cyclically. The resulting contraction and expansion of the muscle fiber is shown, alongside the variation of the normalized contractile element's length, in **Figure 28**.

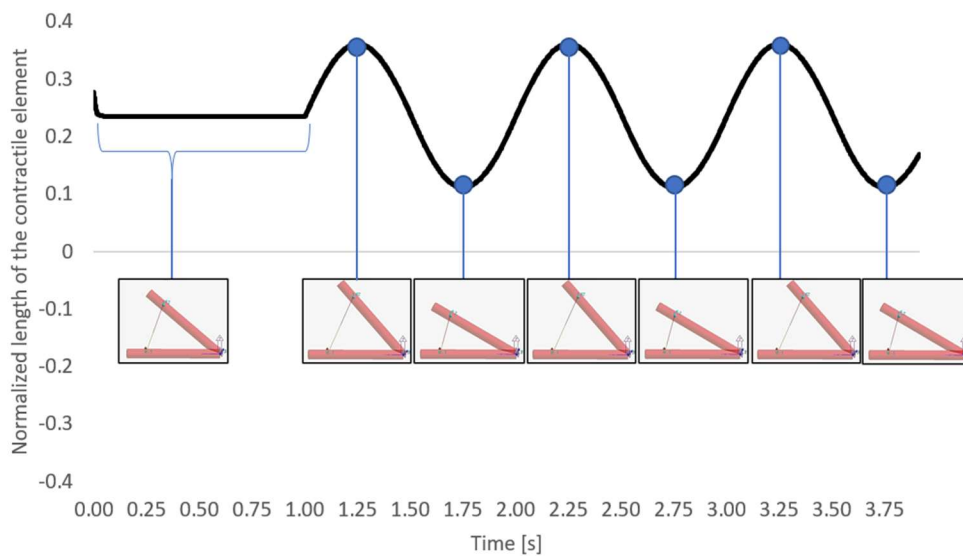


Figure 28 Cyclic contraction and expansion of the muscle fiber attached to two segments due to external activation

The resulting normalized force components of serial element (f_{SE}), contractile element (f_{CE}) and parallel element (f_{PE}) are plotted along with the normalized change in the length of the contractile element (l_{CE}) against time in **Figure 29**.

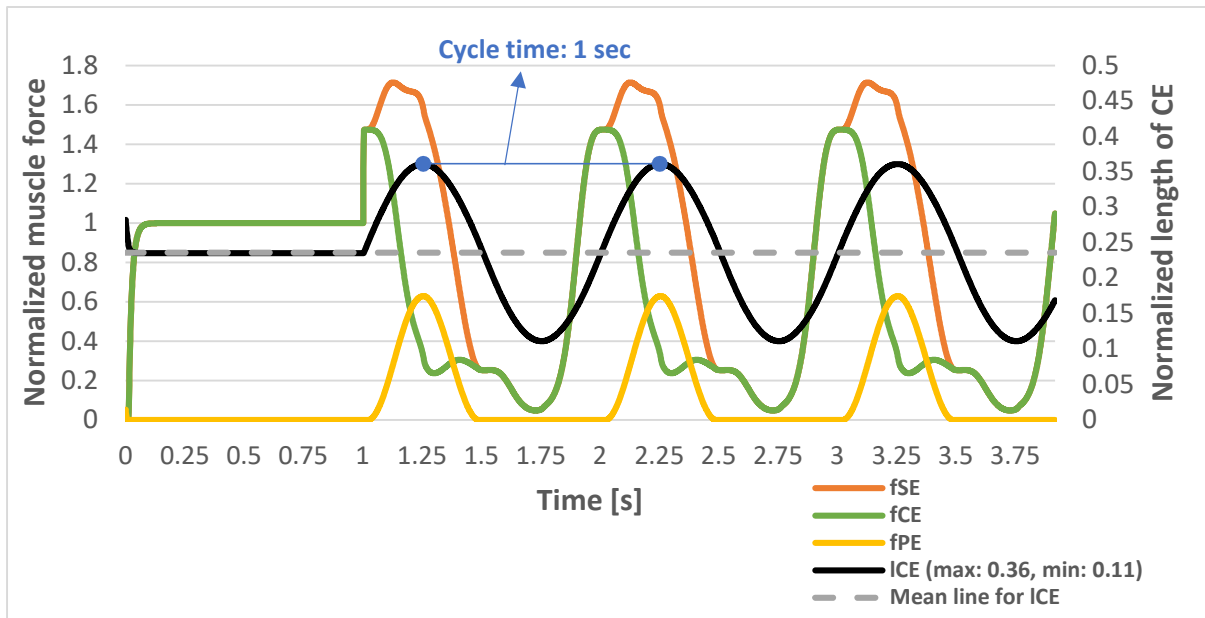


Figure 29 Normalized muscle component forces f_{SE} , f_{CE} and f_{PE} along with the variation in the length of contractile element plotted against time.

The contractile element reaches a maximum normalized length of 0.36 and a minimum of 0.11. A mean line is plotted at 0.235 to observe the oscillations and isolate one cycle. The distance between two adjacent crests, for l_{CE} , is 1 second. The portion of data between two adjacent crests of l_{CE} is plotted in **Figure 30**.

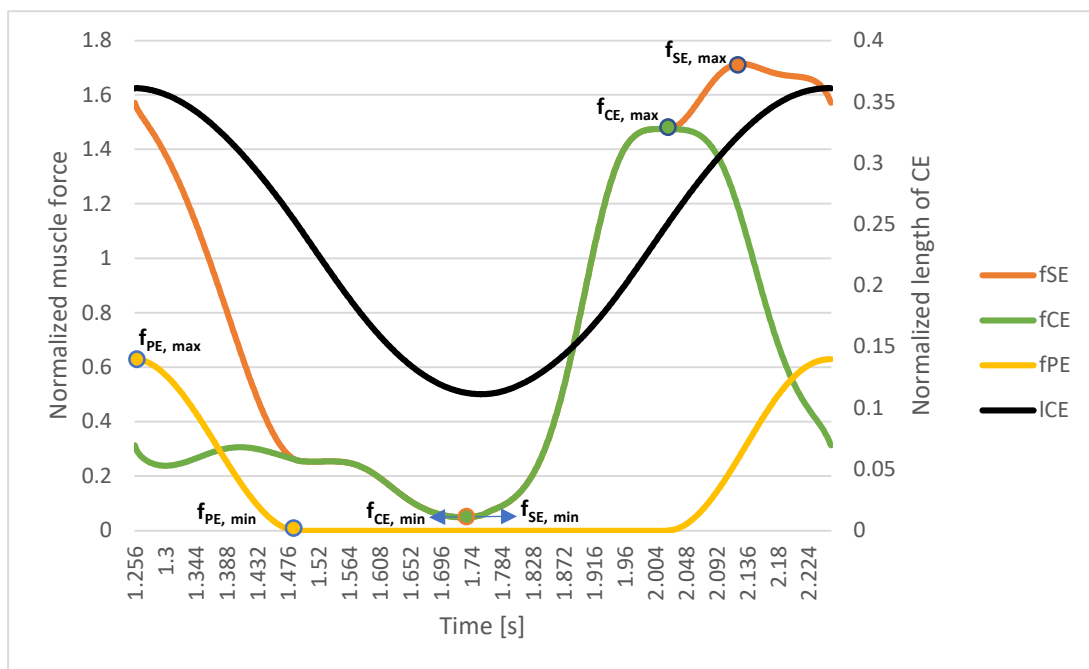


Figure 30 f_{SE} , f_{CE} , f_{PE} and l_{CE} plotted for one cycle of contraction and expansion. The minimum value of f_{CE} coincides with that of f_{SE}

The crest and troughs values of each of the component presented above have been described in **Table 15**.

Table 15 Maximum and minimum values of f_{SE} , f_{CE} , f_{PE} and l_{CE} found from the simulation

Parameter	Minimum	Maximum
l_{CE}	0.11	0.36
f_{SE}	0.05	1.71
f_{CE}	0.05	1.47
f_{PE}	0.00	0.63

4.4 Monoarticular muscle output parameters from the simulations

In this section, the monoarticular muscles have been tested. All five monoarticular muscles have been tested using Newton-Raphson method (section 3.6.1)., while the HFL muscle has been tested also with the velocity integration method (section 3.6.2). Then the effect of shifting the origin of muscles and changing the actuation delay has been shown for muscles computed according to Newton-Raphson method.

4.4.1 Output of the five monoarticular muscle groups using length integration method

The five monoarticular muscle groups were given an activation of 1 in separate simulations and the output values of force and length of the contractile element obtained from the algorithm based on CE length integration (refer to section 3.6.1) were recorded.

The muscle attaches segments at origin and insertion points. In these simulations, origin and insertion coordinates are chosen to provide an actuation of the lower limbs. The Z coordinate of the origin points of all the muscle groups have been offset by a value of 0.07 m from the insertion points order in to produce torque and prevent compressive action. The origin and insertion points of the eight muscle groups and the segments they are attached to are given in **Table 16**.

Table 16 Origin and insertion points along of the eight muscle groups along with the segments which they attach. The coordinates X (horizontal), Y (vertical) and Z (through screen) are measured from the centre of mass of the segments which the muscles attach.

Muscle group	Segment 1	Distance from segment 1's COM [m]			Segment 2	Distance from segment 2's COM [m]		
		X ₁	Y ₁	Z ₁		X ₂	Y ₂	Z ₂
SOL	Low leg	-0.09	0	0.05	Plantar	0	0.01	0
TA	Low leg	-0.12	0	-0.05	Plantar	0	-0.08	0
GAS	Up leg	0	0	0.07	Plantar	0	0	0
VAS	Up leg	-0.15	0	0.06	Low leg	0	0	0
HAM	Hip	-0.07	0	0.07	Low leg	0	0	0
RF	Hip	-0.07	0	0.07	Low leg	0	0	0
GLU	Hip	-0.07	0	0.14	Up leg	0.04	0	0
HFL	Hip	-0.07	0	-0.12	Up leg	0.04	0	0

SOL is a monoarticular muscle providing actuation to bend the feet forward, as shown in **Figure 31**.

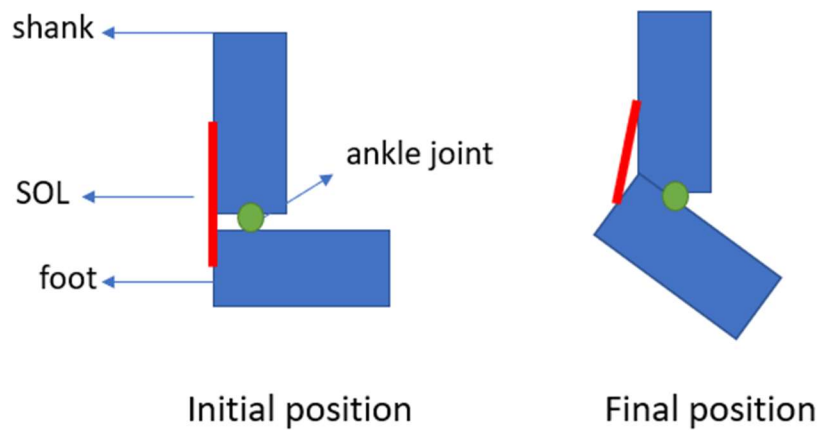


Figure 31 Initial and final position of the leg after activating the SOL muscle

The effect of an giving an activation equal to 1 to the SOL muscle sees a steady drop in the length of the contractile element, which stabilises when it reaches 0.17 m. The contractile force reaches a maximum of 277 N and maintains a steady 100 N towards the end of the cycle which can be observed in **Figure 32**.

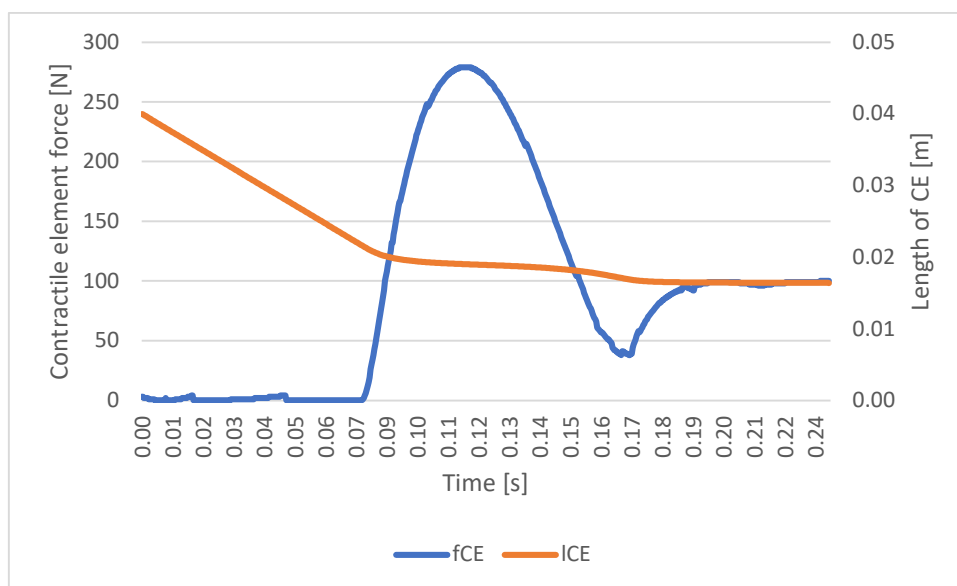


Figure 32 Force exerted by the SOL muscle group's contractile element plotted with length of CE due to activation of value 1

When the TA muscle group is activated, it expresses a similar behavior as the SOL group but helps bend foot upwards as shown in **Figure 33**.

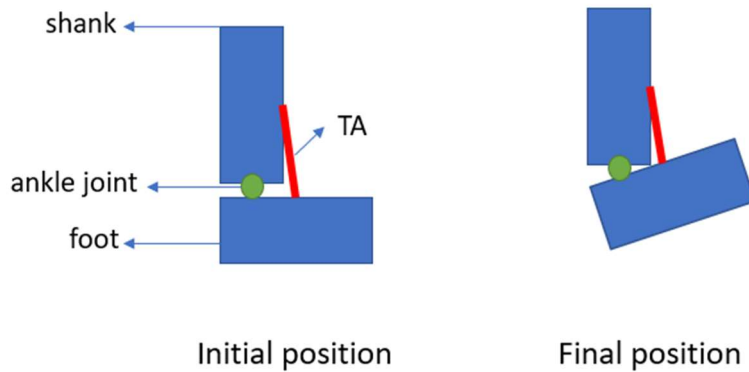


Figure 33 Initial and final position of the leg after activating the TA muscle

The contractile element steadily drops and reaches a length of 0.025 m in a very short period of time as the initial position is very close to the final one. Beyond this point any additional activation will cause the foot to twist along the ankle. This behavior can be observed in **Figure 34**. When the minimum length is reached the contractile element starts exerting force

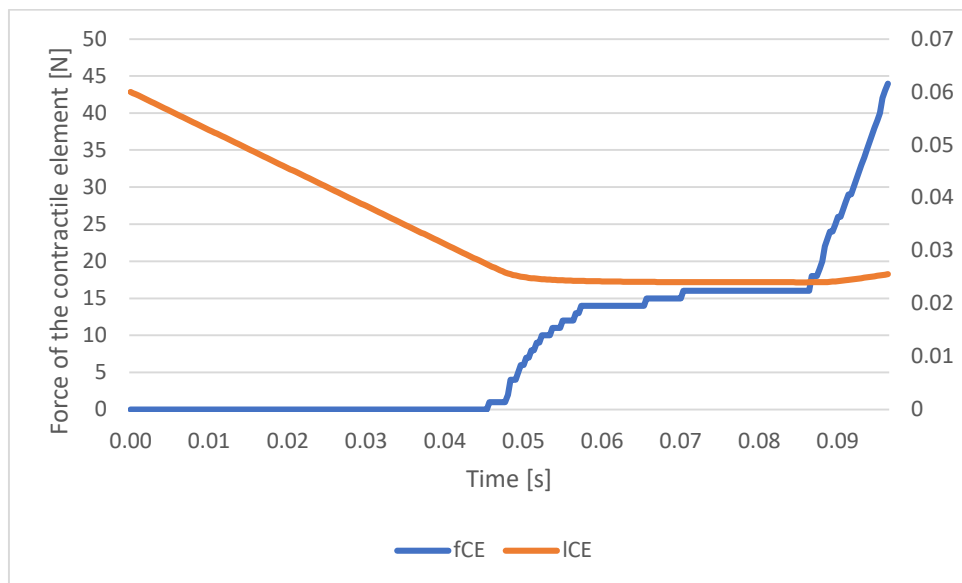


Figure 34 Force exerted by the TA muscle group's contractile element plotted with length of CE due to an activation of value 1

The VAS group, when activated, bends the shank upwards and closer to the thigh as shown in **Figure 35**. Due to the weight of the shank and the foot, the force applied is higher. The origin point is offset with respect to the insertion point in order to generate sufficient bending torque at the knee.

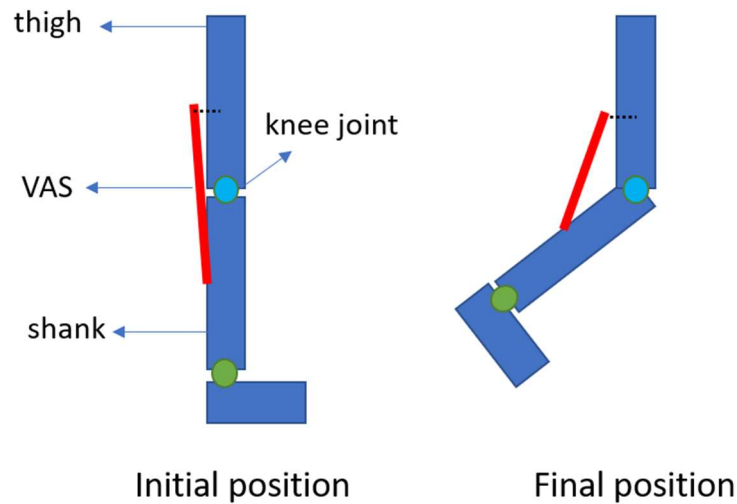


Figure 35 Initial and final position of the leg after activating the VAS muscle. The black dotted line used to denote the distance of the origin point from the centre of mass of the segment

The contractile element's length drops as the leg bends, becoming less steep after reaching a value of 0.05 m. The force steeply increases at this point and gradually drops. This behavior can be observed in **Figure 36**.

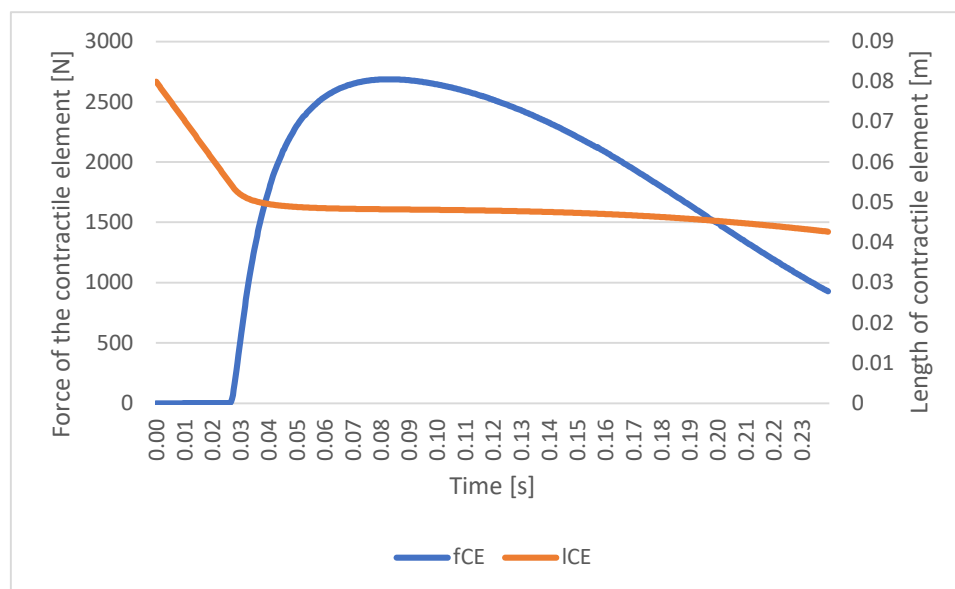


Figure 36 Force exerted by the VAS muscle group's contractile element plotted with length of CE due to activation of value 1

The GLU muscle undergoes very little contraction, but lifts the entire leg, hence the force it exerts is high. The schematic of GLU muscle group, in action, is described in **Figure 37**.

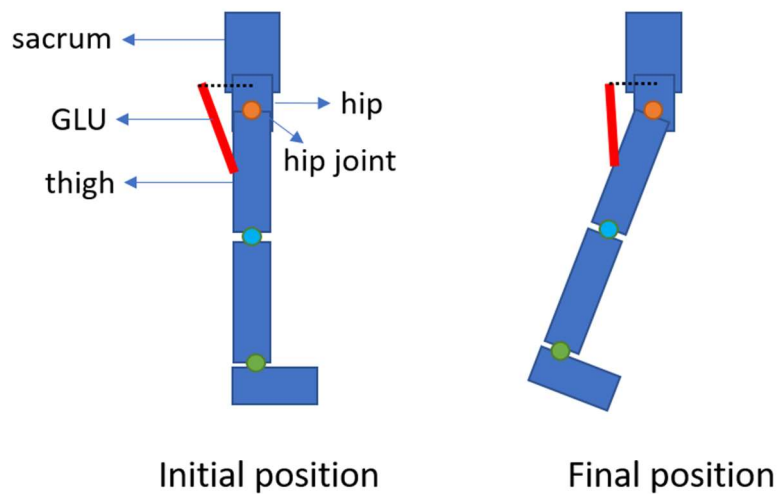


Figure 37 Initial and final position of the leg after activating the GLU muscle. The black dotted line used to denote the distance of the origin point from the centre of mass of the segment

The force applied by the contractile element of GLU group climbs during activation and drops afterwards. It has a high magnitude, close to the maximum possible isometric force of 1500 N, as the entire leg has to be lifted. The length of CE gradually decreases throughout the cycle and reaches 0.08 m towards the end. This trend can be observed in **Figure 38**.

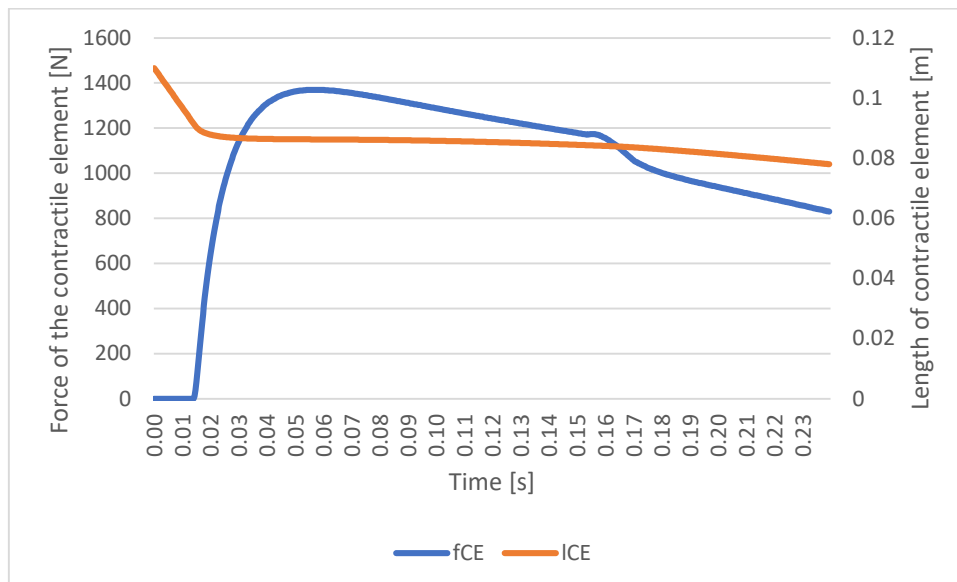


Figure 38 Force exerted by the GLU muscle group's contractile element plotted with length of CE due to activation of value 1

The HFL group attaches the hip to the upper leg and is the counter part of GLU. It applies force to lift the leg forward and up. This muscle too needs to apply enough force to lift the entire leg. This can be observed in the schematic described in **Figure 39**.

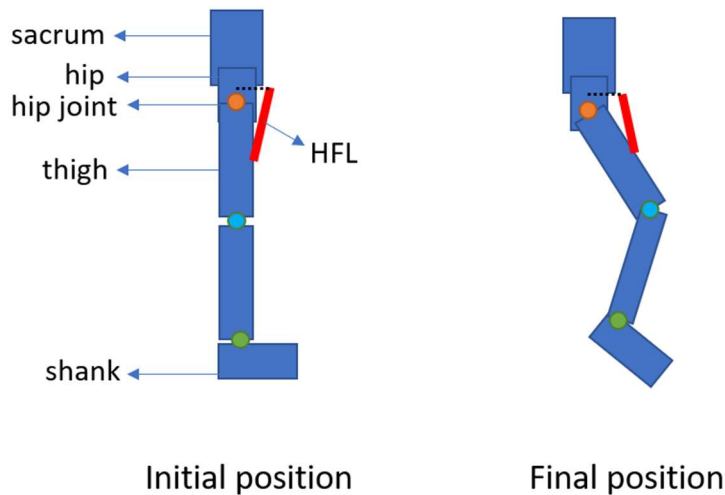


Figure 39 Initial and final position of the leg after activating the HFL muscle. The black dotted line used to denote the distance of the origin point from the centre of mass of the segment

The length of the contractile element of the HFL group steadily drops during the activation. The force it exerts climbs to 1600 N in the beginning of the simulation and continues to drop. This can be observed in **Figure 40**.

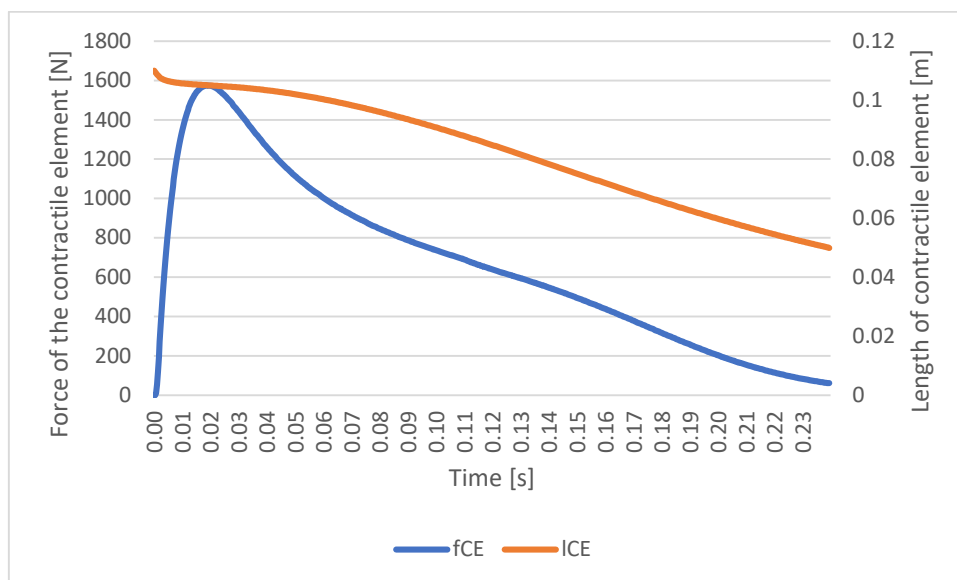


Figure 40 Force exerted by the HFL muscle group's contractile element plotted with length of CE due to activation of value 1

4.4.2 Output of HFL using velocity integration method

HFL muscle group was given an activation of 1 and the output values of force and length of the contractile element obtained from the algorithm based on CE velocity (see section 3.6.2) integration was recorded.

The initial conditions of the muscle are as follows:

- $l_{CE} = l_{opt}$ (for HFL)
- $v_{CE} = 0$ m/s (contraction velocity of the muscle)
- Hip angle = 175°

The output force of the musculotendon unit (f_{mtu}) and the length of the contractile element (l_{CE}) are plotted in **Figure 41**.

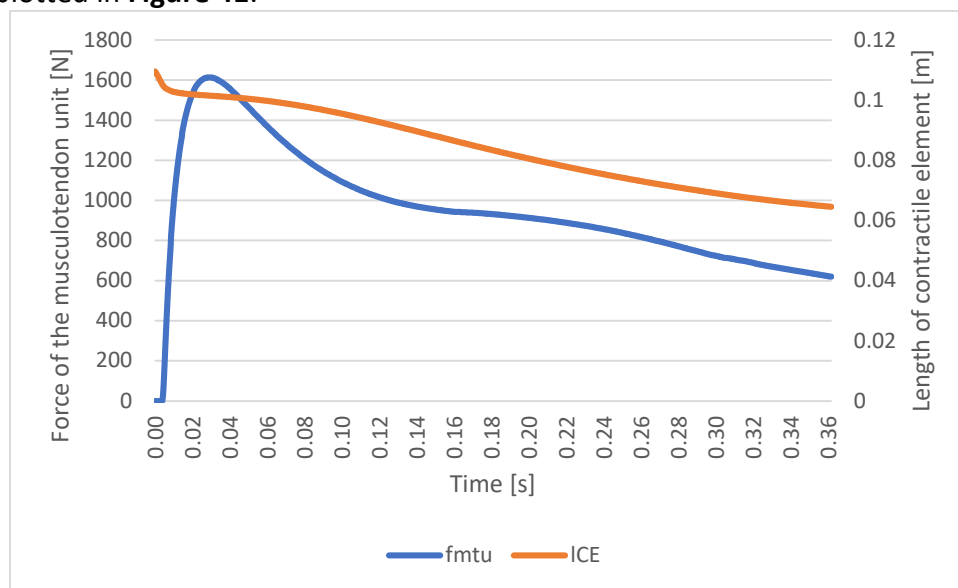


Figure 41 Force exerted by HFL musculotendon unit and the length of its contractile element plotted against time, computed using velocity integration method

The trend of the force exerted and length of the CE computed with velocity integration method yields results similar to that of length Newton-Raphson method.

4.5 Effect of change in position of the origin point

In this section, the effect of shifting the origin point of muscles developed according to Newton-Raphson method is evaluated.

In previous simulation, the insertion and origin points were chosen in order to fulfil the following criteria:

- The muscle should lift the segments, it is connected to, in a realistic way
- In the preliminary simulation phase, collision/interference of the segments with each other or with the ground has to be avoided
- The maximum force generated by the muscles should be within realistic limits

In order to exhibit the sensitivity of the position of the origin points, simulations were conducted in which its position was changed in the X and Z coordinate directions for the VAS muscle group, as shown in **Figure 42**.

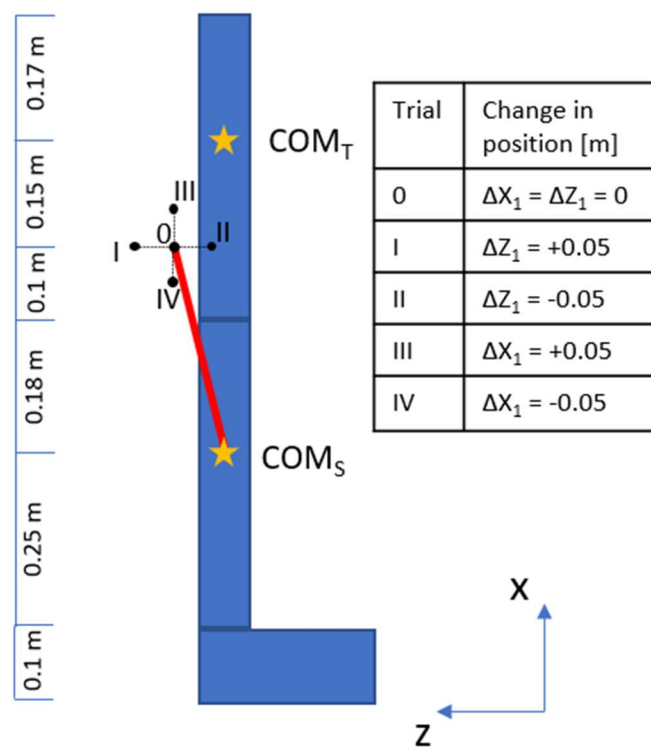


Figure 42 Positions of the origin point of VAS chosen for the four trials. The original origin point has been denoted with position 'O', which is below (X-direction) the centre of mass of the thigh by 0.15 m and behind (Z-direction) by 0.07 m. Note: the coordinate system mentioned in this figure is tilted when compared to the global coordinate system as the upper and lower leg segments are rotated by 90° during their creation. COM_T and COM_S denote the centre of mass position of the thigh and the shank respectively.

Length and force values of the contractile element when the origin point is moved behind the original position (by 5 cm in Z direction) have been described in **Figure 43**.

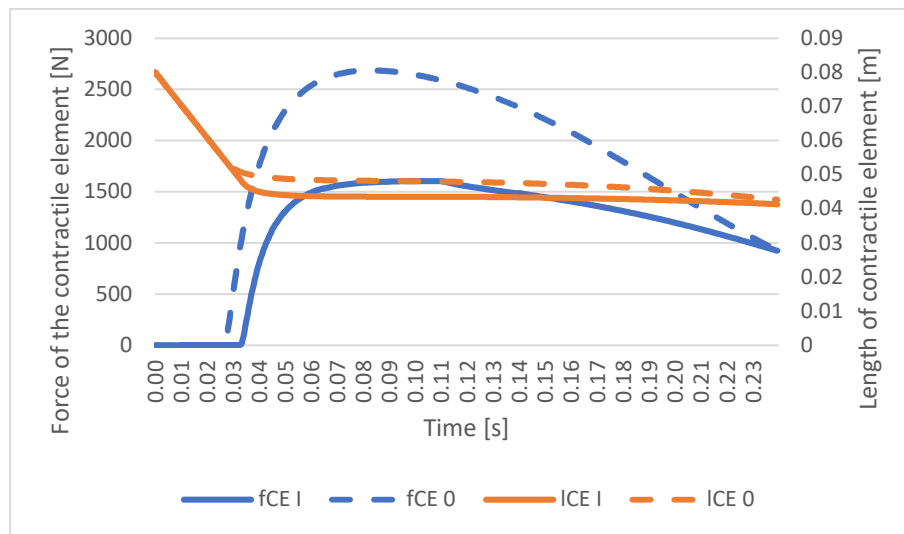


Figure 43 VAS muscle’s contractile element (CE) force and length comparison when the origin point is behind by 5 cm (in the Z direction). The values of forces and lengths for of the CE for the original trial ‘0’ have been plotted as dotted lines.

The maximum force exerted by the CE has dropped by 1000 N while the difference in the trend of the length of the contractile element is marginal when compared to the original case.

The values of force and length of CE when the origin point is moved closer to the segment (by 5 cm in Z direction) have been plotted in **Figure 44**.

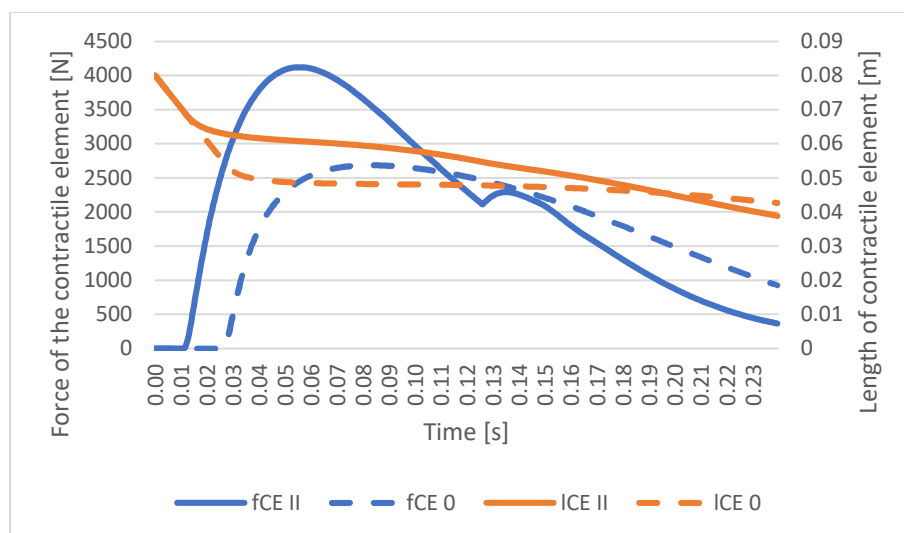


Figure 44 VAS muscle’s contractile element (CE) force and length when the origin point is closer to the thigh (by 5 cm in Z direction) compared to the original position. The values of forces and lengths for of the CE for the original trial ‘0’ have been plotted as dotted lines.

The trend of length of CE drops less steeply at the beginning and curves down to the value obtained at the end of the original case. The maximum force exerted by CE reaches maximum, of 4000 N, earlier when compared to the original case’s 2600 N.

Length and force exerted by the contractile element when the origin point is moved above the original position (by 5 cm in X direction) have been described in **Figure 45**.

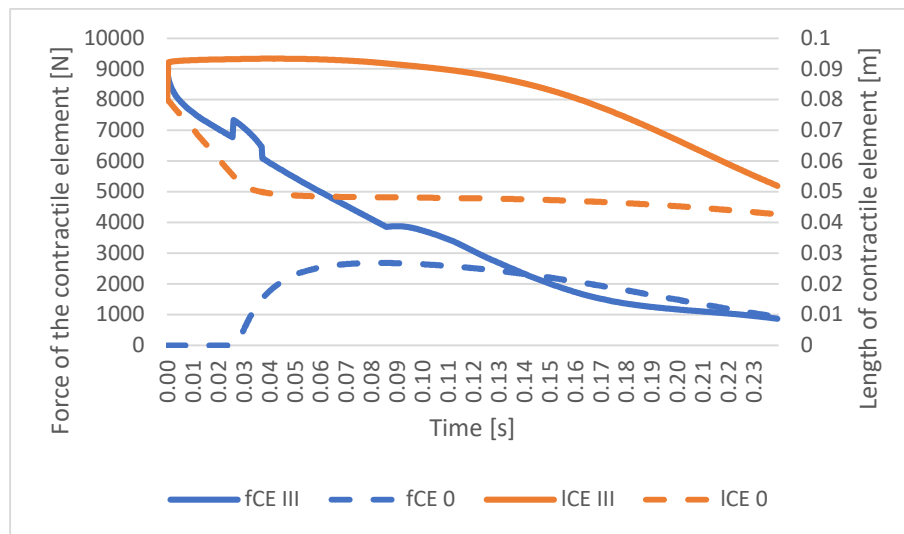


Figure 45 VAS muscle's contractile element (CE) force and length when the origin point is moved up by 5 cm in the X direction. The values of forces and lengths for of the CE for the original trial '0' have been plotted as dotted lines.

The maximum force of CE is three times that of the original value. The length shoots up to almost 0.09 m and gradually drops for the rest of the simulation.

Length and force exerted by the contractile element, when the origin point is moved below the original position (by 5 cm in X direction), have been described in **Figure 46**.

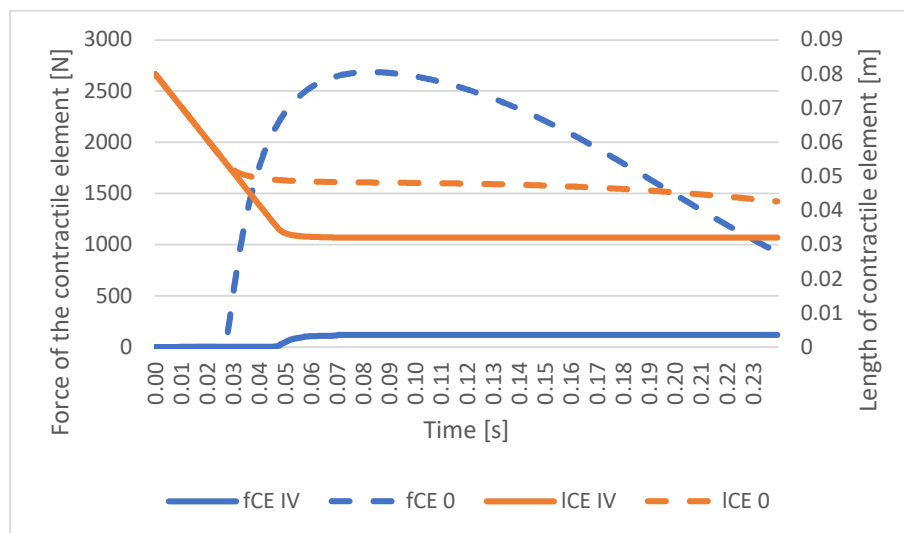


Figure 46 VAS muscle's contractile element (CE) force and length when the origin point is below the original position by 5 cm (in the X direction). The values of forces and lengths for of the CE for the original trial '0' have been plotted as dotted lines.

The maximum force exerted by the CE is only 120 N when compared to the original case in which it was almost 2600 N. The length of CE drops and settles at 0.03 m, a length lower than that obtained in the original case.

The values of maximum force of the CE and the length at the end of the simulation have been mentioned in **Table 17**.

Table 17 Maximum value of force of CE and length of CE at the end of the simulation for the trials I-IV in which the origin point's position was moved in different directions

Trials	Maximum f_{CE} [N]	Value of l_{CE} at the end of the simulation [m]
0 (original)	2686	0.04
I	1605	0.04
II	4121	0.04
III	8936	0.05
IV	118	0.03

The maximum force exerted by CE is lower than that of the original trial for trial I as the origin point moves away from the insertion point. In trial II, as the origin point moves closer to the thigh segment, a notable increase in force can be observed. For trial III, the maximum force exerted by CE is the largest as the origin point moves away from the insertion point along the X direction. Trial IV has the smallest maximum force exerted by CE as the origin point is closest to the insertion point.

Changing the origin point of VAS muscle in the X direction has a considerable change in the output forces, whereas change in Z direction has only a minor change in muscle output. In order to demonstrate the sensitivity of change of the origin point in X direction, we conduct two more trials in which the point is displaced by 0.5 cm in the positive and negative X direction.

4.6 Effect of delay between nervous excitation and muscular activation

There is a delay between the nervous excitation and muscular activation governed by the following equation:

$$a_i = 100 \times s \times (e_i - a_{i-1}) + a_{i-1} \quad (20)$$

Where a_i is the activation for the current time frame, s is the step size, a_{i-1} is the activation for the previous time frame and e_i is the nervous excitation for the current frame. When step size is $1/100$ s, there is no delay between the excitation and activation. This delay's effect is significant especially for low values of step size. The delay between nervous excitation and muscular activation for a step size of $1/10000$ s is plotted in **Figure 47**.

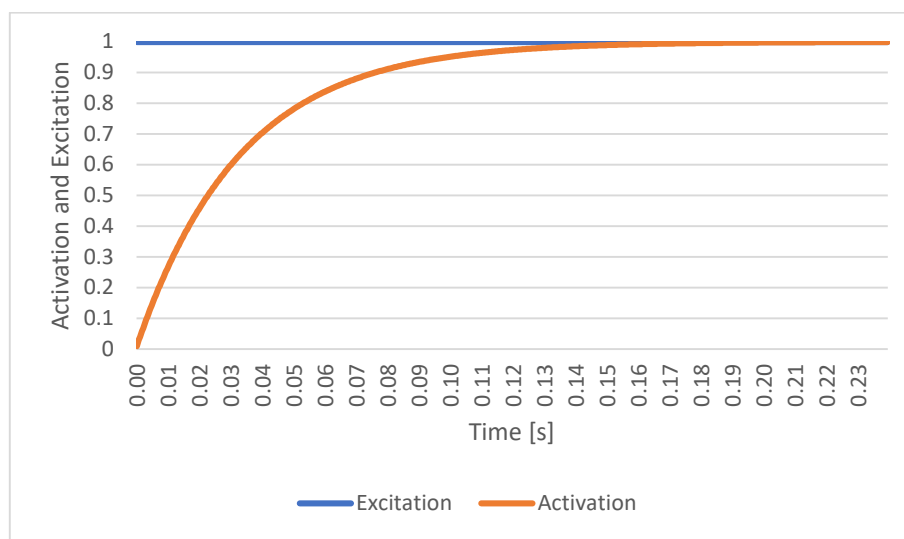


Figure 47 Nervous excitation and muscular activation for a step size of $1/10000$ s.

When VAS muscle group is given nervous excitation with a step size of $1/10000$ s, the effect on the muscle forces exerted by the contractile element is as shown in **Figure 48**. A difference in the trend of f_{CE} can be seen due to the added delay. The force drops slower towards the second half of the simulation.

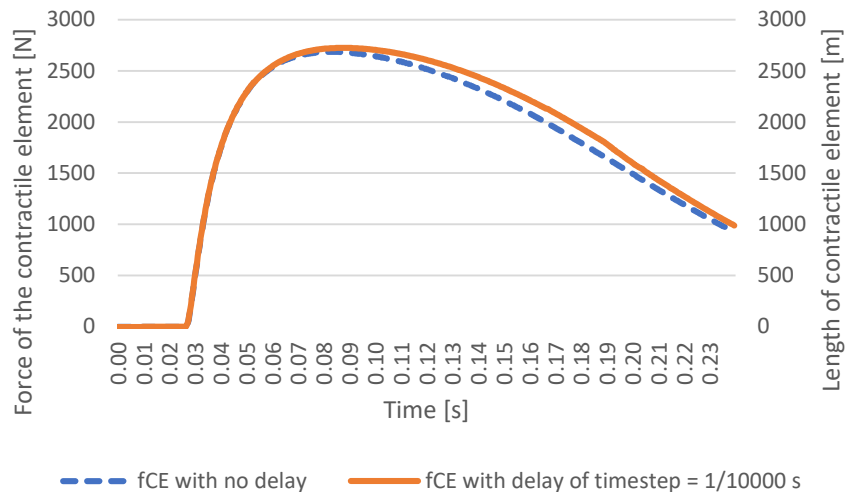


Figure 48 Force exerted by VAS contractile element plotted, for a step size of $1/10000$ s. The dotted line indicates the curve of f_{CE} when there is no delay.

The output length of the contractile element is shown in **Figure 49**. The trend followed by the length of CE is nearly identical except the delay causes the length to drop slower towards the later part of the simulation.

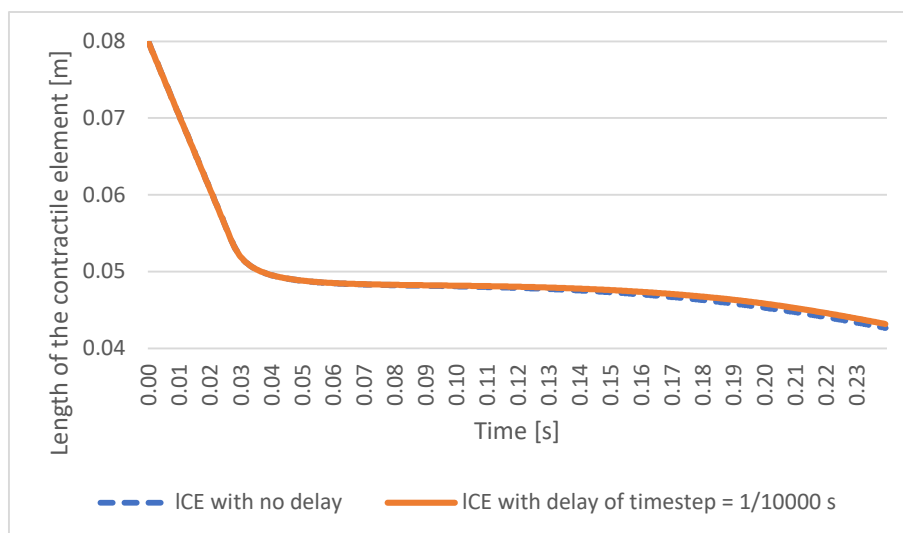


Figure 49 Length of VAS' contractile element plotted for a step size of $1/10000$ s. The dotted line indicates the curve of l_{CE} when there is no delay.

The effect of delay in nervous excitation and muscular activation does not have a significant change for longer periods of activation as the forces catch up eventually. When the fluctuation in excitation is more rapid, this delay will have a more pronounced effect on the forces exerted by the muscle.

Chapter 5: Conclusions and future developments

5.1 Conclusions

To study the effect of mediolateral vibrations on human body, a musculoskeletal model has been implemented in a real-physics simulation environment. A suitable simulation environment have been selected, anthropometric data has been retrieved from literature and two type of muscle force computation have been tested.

Anthropometric data such as the segment lengths, masses and inertias were collected from various literature sources and compared. The inertia and mass of the trunk varied among the sources as some models' trunk included the hand, head and the pelvis while others did not. The coordinate system adapted to describe the inertia of the model, in three directions, varied from author to author. Data from three different sources have been compared and data given by de Leva [34] have been selected because they are used in biomechanical studies and because they were in accordance with the other two authors. The anthropometric data used in this study is easily editable for different subjects and is accessed from an XML file (data are written in Appendix).

The lower limbs have been actuated by 8 type-Hill muscles. Suitable muscle parameters have been retrieved from literature. The Hill-Type model has been tested in two different configurations and approaches. The first method solved the internal degree of freedom of the muscle using internal state variable to perform Newton-Raphson algorithm. The second muscle model instead, solved the internal degree of freedom by numerical integration of the contraction velocity of the muscle. The force given by the HFL muscle obtained from both methods are comparable in terms of maximum force (1600 N) and response time (200 ms for the integration method and 400 ms for the Newton-Raphson method to reach the maximum force). Also, the length contraction was similar for both methods and equal to 5 cm. These results are in accordance with Van Leeuwen findings [43].

The literature lacks information of the origin and insertion points of the muscle groups. So, for Newton-Raphson method, the origin points of the muscles were adjusted to produce the actuation of the lower limbs. Variation of origin point of the muscles have been investigated. In addition, the effect of delay between the nervous excitation and muscular activation has a pronounced effect during the scenario of fast fluctuation of excitation or small values of timesteps, but for extended periods of constant excitation, the effect is negligible.

5.2 Limitations and future developments

In this preliminary study, just monoarticular muscles have been tested, a suitable algorithm is needed to calculate the force and length of biarticular muscles. This algorithm should use the contraction velocity integration method. In fact, the Newton-Raphson method cannot take in account the sliding of the biarticular muscle on one joint in the computation of the muscle length. To find the best origin and insertion points, an optimization approach should be used. The type Hill's muscle model is widely used for human gait simulations but does not account for the change in the muscular properties due to fatigue.

The next step will be to add a control strategy based on muscle metabolic expenditure and walking speed. The model will be trained using a machine learning model to achieve a certain stride speed or metabolic efficiency. Then, the model will be exposed to oscillations in the medio-lateral plane to study the effects of medio-lateral vibrations while walking.

Bibliography

- [1] Bovenzi, M., "A longitudinal study of low back pain and daily vibration exposure in professional drivers" *Industrial Health*, vol. 48, pp. 584–595, 2010.
- [2] Donati, P., "Workplace exposure to vibration in Europe: an expert review," *Off. Off. Publ.*, vol. 215, no. 4, pp. 947–957, 2008.
- [3] Nordlund, M. M., and Thorstensson, A., "Strength training effects of whole-body vibration?" *Scandinavian Journal of Medicine and Science in Sports*, 2007.
- [4] Lam, T. P., Ng, B. K. W., Cheung, L. W. H., Lee, K. M., Qin, L., Cheng, J. C. Y., "Effect of whole body vibration (WBV) therapy on bone density and bone quality in osteopenic girls with adolescent idiopathic scoliosis: A randomized, controlled trial," *Osteoporos. Int.*, 2013.
- [5] Naón, M. G., Tarabini, M., Marzaroli, P., Marelli, S., Moorhead, A. P., "The effects of mediolateral vibrations while walking on a treadmill: a setup for cognitive task and gait analysis," 2020.
- [6] Matsumoto, Y., Griffin, M. J., "Mathematical models for the apparent masses of standing subjects exposed to vertical whole-body vibration". *Journal of Sound and Vibration*, 260(3), 431–451. [https://doi.org/10.1016/S0022-460X\(02\)00941-0](https://doi.org/10.1016/S0022-460X(02)00941-0), 2003.
- [7] Subashi, G. H. M. J., Matsumoto, Y., & Griffin, M. J., "Modelling resonances of the standing body exposed to vertical whole-body vibration: Effects of posture". *Journal of Sound and Vibration*, 317(1–2), 400–418. <https://doi.org/10.1016/j.jsv.2008.03.019>, 2008.
- [8] Chadeaux, D., Goggins, K., Cazzaniga, C., Marzaroli, P., Marelli, S., Katz, R., Eger, T., Tarabini, M., "Development of a two-dimensional dynamic model of the foot-ankle system exposed to vibration," *Journal of Biomechanics*, 99, 109547, 2020.
- [9] Baker R., Leboeuf F., Reay J., Sangeux M., "The Conventional Gait Model - Success and Limitations". In: Müller B., Wolf S. (eds) *Handbook of Human Motion*. Springer, Cham. https://doi.org/10.1007/978-3-319-14418-4_25, 2018.
- [10] Leboeuf, F., Baker, R., Barré, A., Reay, J., Jones, R., Sangeux, M., "The conventional gait model, an open-source implementation that reproduces the past but prepares for the future", *Gait & Posture*, 69, 235–241. <https://doi.org/10.1016/j.gaitpost.2019.04.015>, 2019.
- [11] Vicom Motion Systems (2021) Nexus [Software package] <https://www.vicon.com/software/nexus/>
- [12] Kainz, H., Graham, D., Edwards, J., Walsh, H. P. J., Maine, S., Boyd, R. N., Lloyd, D. G., Modenese, L., Carty, C. P., "Reliability of four models for clinical gait analysis," *Gait & Posture* 54, 2017.
- [13] Wang, J. M., Hamner, S. R., Delp, S. L., Koltun, V., "Optimizing locomotion controllers using biologically-based actuators and objectives," *ACM Transactions on Graphics*, 31(4), <https://doi.org/10.1145/2185520.2185521>, 2012.

- [14] Millard, M., McPhee, J., Kubica, E., “Multi-step forward dynamic gait simulation”, *Computational Methods in Applied Sciences*, 12, 25–43, 2009.
- [15] Zadpoor, A. A., Nikooyan, A. A. “Modeling muscle activity to study the effects of footwear on the impact forces and vibrations of the human body during running,” *J. Biomech.*, 2010.
- [16] MSC Software (2021) ADAMS [Software]. <https://www.mscsoftware.com/product/adams>
- [17] Kia, M., Stylianou, A. P., Guess, T. M., “Evaluation of a musculoskeletal model with prosthetic knee through six experimental gait trials”, *Medical engineering & physics*, 36(3), 335-344, 2014.
- [18] AnyBody Technology A/S (2021) AnyBody [Software]. <http://www.anybodytech.com/>
- [19] Brunner, R., Dreher, T., Romkes, J., Frigo, C., “Effects of plantarflexion on pelvis and lower limb kinematics”, *Gait and Posture*, 28(1), 150–156. <https://doi.org/10.1016/j.gaitpost.2007.11.013>, 2008.
- [20] Design Simulation Technologies (2021) SimWise – 4D [Software]. <https://www.design-simulation.com/SimWise4d/>
- [21] Sherman, M., (2011). Simbody Guide [Source code]. <https://simtk.org/projects/simbody>
<https://simtk.org/docman/view.php/47/1592/SimbodyAndMolmodelUserGuide.pdf>
- [22] Sherman, M. A., Seth, A., Delp, S. L., “Simbody: Multibody dynamics for biomedical research”, *Procedia IUTAM*, 2, 241–261. <https://doi.org/10.1016/j.piutam.2011.04.023>, 2011.
- [23] Simbios (2021) OpenSim [Source code]. <https://simtk.org/projects/opensim/>
- [24] Smith, R., (2021) Open Dynamics Engine [Source code]. <http://www.ode.org/>
- [25] Yin, K., Loken, K., Van De Panne, M., “SIMBICON: Simple biped locomotion control”, *ACM Transactions on Graphics* 26, 3 (July), 105, 2007.
- [26] Julio, J., Alain, S., (2021) Newton Dynamics (3.14) [Source code]. <http://newtondynamics.com>
- [27] Lee, T., (2021) TinyXML (2.5.3) [Source code]. <http://www.grinninglizard.com/tinyxml/>
- [28] Omar, C., (2021) Dear ImGui (1.50) [Source code]. <https://github.com/ocornut/imgui>
- [29] Milan, I., Marcelo, M., (2021) OpenGL Extension Wrangler Library (2.1.0) [Source code]. <https://github.com/nigels-com/glew>
- [30] The GLFW Development Team (2021) GLFW (3.3) [Source code]. <https://github.com/glfw/glfw>
- [31] G-Truc Creation (2021) GLM (0.9.9) [Source code]. <https://github.com/g-truc/glm>

- [32] Dempster, W. T., Gaughran, G. R. L., "Properties of body segments based on size and weight," *Am. J. Anat.*, 1967.
- [33] Zatsiorsky, V., "Kinematics of Human Motion," Human Kinetics Publishers, 2002.
- [34] de Leva, P., "Technical Note: Adjustment to Zatsiorsky-Seluyanov's segment inertia parameters," *J. Biomechanics*, vol. 29, no. 9. pp. 1223–1230, 1996.
- [35] Dumas, R., Chèze, L., Verriest, J. P., "Adjustments to McConville et al. and Young et al. body segment inertial parameters," *J. Biomech.*, vol. 40, no. 3, pp. 543–553, 2007.
- [36] Hanavan, E. P., "A mathematical model of the human body," AMRL-TR-64-102.AMRL TR, 1964.
- [37] Wooten, W. L., Hodgins, J. K., "Animation of human diving," *Comput. Graph. Forum*, vol. 15, no. 1, pp. 3–13, 1996.
- [38] Geyer, H., & Herr, H., "A Muscle-reflex model that encodes principles of legged mechanics produces human walking dynamics and muscle activities", *IEEE Transactions on Neural Systems and Rehabilitation Engineering*, 18(3), 263–273, 2010.
- [39] Frigo, C. A., Wyss, C., Brunner, R., "The effects of the rectus femoris muscle on knee and foot kinematics during the swing phase of normal walking", *Applied Sciences (Switzerland)*, 10(21), 1–12. <https://doi.org/10.3390/app10217881>, 2020.
- [40] Winter, D. A., *Biomechanics and Motor Control of Human Movement: Fourth Edition*. In *Biomechanics and Motor Control of Human Movement: Fourth Edition*. <https://doi.org/10.1002/9780470549148>, 2009.
- [41] Yamaguchi, G. T., Sawa, A. G. U., Moran, D. W., Fessler, M. J., Winters, J. M., "A survey of human musculotendon actuator parameters," in *Multiple Muscle Systems: Biomechanics and Movement Organization*, J. Winters and S.-Y. Woo, Eds. New York: Springer-Verlag, pp. 717–778, 1990.
- [42] Riener, R., & Fuhr, T., Patient-driven control of FES-supported standing up: A simulation study. *IEEE Transactions on Rehabilitation Engineering*, 6(2), 113–124. <https://doi.org/10.1109/86.681177>, 1998.
- [43] Van Leeuwen, J. L. "Muscle function in locomotion." *Mechanics of animal locomotion* 11 (1992): 191-249.

Appendix

Input XML file containing the muscle and body segment data

```
<?xml version="1.0" ?>
<Model>
  <!-- Parameters for musculoskeletal model -->
  <Parameters>
    <!--Scaling factor of length and mass-->
    <Scale length ="1.0" mass ="1.0"/>
    <!-- Lengths in m, Weight in kg, Masses in % of Weight, Inertia
    in Radius of gyration in % of Weight, COM in % (starting from
    proximal point of each segment) of length, Angles in degrees,
    Insertion Points' distances in m (starting from COM) -->
    <Lengths UpLeg="0.4222" LowLeg="0.4340" Plantar="0.183"
    Spine="0.3862" UpArm="0.28" LowArm="0.27" Hand="0.0862"
    Head="0.2033" Hip="0.15" Sacrum="0.1457" Toe="0.06" Foot="0.1"
    Neck="0.0396" Clav="0.225" RBones ="0.07" />
    <Weight value="73.0"/>
    <Masses head="0.0694" trunk="0.4346" uparm="0.0271"
    forearm="0.0162" hand="0.0061" thigh="0.1416" shank="0.0433"
    foot="0.0137"/>
    <Inertia>
      <Ixx head="0.362" trunk="0.372" uparm="0.285" forearm="0.276"
      hand="0.628" thigh="0.329" shank="0.255" foot="0.257" />
      <Iyy head="0.376" trunk="0.347" uparm="0.269" forearm="0.265"
      hand="0.513" thigh="0.329" shank="0.249" foot="0.245" />
      <Izz head="0.312" trunk="0.191" uparm="0.158" forearm="0.121"
      hand="0.401" thigh="0.149" shank="0.103" foot="0.124" />
    </Inertia>
    <COM head="0.5976" trunk="0.4486" uparm="0.5772" forearm="0.4574"
    hand="0.7900" thigh="0.4095" shank="0.4459" foot="0.4415" />
    <Angles hip="-30.0" clav="0.0" />
    <MuscleInsertionPoints>
      <X1 sol="-0.09" ta="-0.12" gas="0" vas="-0.15" ham="-0.075"
      rf="-0.075" glu="-0.075" hfl="-0.075"/>
      <Y1 sol="0" ta="0" gas="0" vas="0" ham="0" rf="0" glu="0"
      hfl="0"/>
      <Z1 sol="0.05" ta="-0.05" gas="0.07" vas="0.06" ham="0.07"
      rf="0.07" glu="0.14" hfl="-0.12"/>
      <X2 sol="0" ta="0" gas="0" vas="0" ham="0" rf="0" glu="0.04"
      hfl="0.04"/>
      <Y2 sol="0.01" ta="-0.08" gas="0" vas="0" ham="0" rf="0"
      glu="0" hfl="0"/>
      <Z2 sol="0" ta="0" gas="0" vas="0" ham="0" rf="0" glu="0"
      hfl="0"/>
    </MuscleInsertionPoints>
    <MaxMuscleForce sol="4000" ta="800" gas="1500" vas="6000"
    ham="3000" rf="1000" glu="1500" hfl="2000"/>
  </Parameters>
</Model>
```